

1057

1057

37

SMITH MULTIMODULE SOLAR-ELECTRIC PLANT

by

Dr. Otto J. M. Smith
612 Euclid Avenue
Berkeley, California 94708

Copyright, 1975, Otto J. M. Smith

All Patent and Reproduction Rights Reserved

1-7-4

OTTO J. M. SMITH, Ph.D
REGISTERED PROFESSIONAL ENGINEER

Feedback Systems
Industrial Electronics and Controls
Economic Computers

612 Euclid Avenue
Berkeley, California 94708

1.7.9
1.7.8
1.7.9

February 18, 1976

Mr. Clifford S. Selvage
Mail Stop 8180
Sandia Laboratories
East Avenue
Livermore, California 94550

Dear Mr. Selvage:

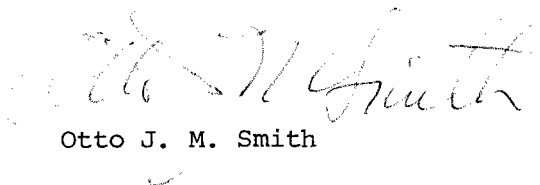
Mr. James Lerner, Special Consultant, Research and Development Division, State of California Energy Resources Conservation and Development Commission, 1111 Howe Avenue, Sacramento, California 95825, has requested me to send directly to you my attached confidential report, "Smith Multimodule Solar-Electric Plant."

In order to protect my patent rights, I request that this material not be published, disclosed to others, or quoted, until after applications for letters of patent have been filed.

This report is being sent to you to facilitate your technical and feasibility evaluations for Mr. Lerner.

In the event that questions arise which you feel could be answered by a conversation, I can be reached at (415) 525-9126 or (415) 642-7591.

Sincerely yours,


Otto J. M. Smith

OJMS:frw

Enclosure

1.7.4

SMITH MULTIMODULE SOLAR-ELECTRIC PLANT

by

Dr. Otto J. M. Smith
612 Euclid Avenue
Berkeley, California 94708

Copyright, 1975, Otto J. M. Smith

All Patent and Reproduction Rights Reserved

SMITH MULTIMODULE SOLAR-ELECTRIC PLANT

Otto J. M. Smith
612 Euclid Avenue
Berkeley, California 94708

A practical solar-thermal-electric power plant can be built at a reasonable cost with available materials and conventional engineering design techniques.

Fields of steerable mirrors concentrate the reflected sunlight on hot receptors behind heat-conserving windows on short towers. The absorbed heat from the hot receptors is carried by heat exchange fluids through pipes to a central station power plant containing heat exchangers to pre-heat and boil water and to superheat steam, a conventional turbine and electrical generator.

A 100-megawatt power plant would be supplied from 1100 towers of 35 meters height, each tower receptor illuminated by a hexagonal field of 50 meters by 48 meters. Each field has 312 mirrors of 2 square meters surface each.

The capital cost in dollars per megawatt-hour of annual production has been reduced by unique heliostat field geometry, mirror construction, high transmission window, high absorption cavity, and optimum utilization of available heat at different temperatures in the thermodynamic cycle.

WINDOW

The high transmission window transmits 96% of the solar energy to the heat receptor. It has at least two panes of low-iron glass, with the space in between the panes filled with triethylene glycol which has essentially the same refractive index as the glass. The reflection from the inside surfaces of the glass is negligible because of the nearly equal refractive indices of the glass and fluid. The triethylene glycol is pumped through the interpane space to provide a cooling effect.

The exterior surfaces of the windowpanes have an antireflection coating of magnesium fluoride.

HEAT RECEPTOR

The incoming light is restricted to a narrow angle by the geometry of the heliostat field. The infrared reradiation from the heat receptor is hemispherical. This difference in angular distribution is utilized to obtain a preferential absorption of solar energy and a low infrared reradiation.

The heat receptor behind the window is an array of stainless pipes coated with intermetallic Al-Cr which has high absorption of solar light at high temperature. Between the main receptor and the window is a grid of intermetallic Al-Ni-coated stainless pipes which have low emissivity for infrared reradiation. The grid is equivalent to plates parallel to the direction of the incoming light. The reradiation primarily from the Al-Ni surfaces at low temperature is reabsorbed by the window. The composite solar absorption of the cavity is 0.997 and the composite infrared emissivity is only 0.4 for radiation from the pipes to the window.

The pipes contain heat-exchange fluids which are pumped at high pressure, high temperature, and high velocity, to abstract the heat from the receptor and carry it back to the heat exchangers in the central power house. A suitable heat exchange fluid is dry steam at 600 pounds per square inch pressure. Leaks are not serious; make-up costs are low; but large pumps (compressors) are required. The steam can be circulated directly through the pebble-bed storage reservoirs, and the low-pressure turbine.

LOSSES

The infrared reradiation from the heat absorbing cavity is absorbed by the low-iron window glass with emissivity of 0.88, and also by the triethylene glycol, which is pumped at a rate sufficient to keep the outside window at a low temperature. Consequently, the infrared losses to the environment are low or negligible, even though the infrared energy delivered to the window from the cavity is appreciable. Likewise, convection heat transfer from the cavity to the window is appreciable, while convection losses to the environment are much less. The triethylene glycol receives enough heat to provide 16% of all the heat needed by the thermodynamic cycle. This heat is pumped into the number one feedwater preheater heat exchanger.

When the TEG (triethylene glycol) pumping rate is too low, the window temperature rises and the heat losses rise. When the TEG pumping rate is too high, the TEG temperature is controlled by the steam cycle. There is an optimum pumping rate which will be controlled by a computer optimization program.

COST SENSITIVITY

A cost analysis of this system shows that the mirror costs are predominant, and that the tower and heat absorber costs are low. A minimum cost design attempts to minimize the cost per KWH of reflected light at the mirrors, and to maximize the efficiency of the system beyond the mirrors, i.e., window, heat cavity, and heat exchangers, even at significantly higher cost for these latter components. When maintenance costs are included, there is an advantage in short towers with small windows and small receptors, and in a distributed system where components can be individually removed from service. Reliability and down time are improved by a modular plant design.

To minimize piping costs, the land utilization ratio is high. This is achieved by an irregular hexagon field shape significantly displaced to the north of the corresponding tower. Each tower is in a field of mirrors concentrating their light on a receptor on a different tower farther south.

MIRRORS

Low cost mirrors are made of flat fiberglass-epoxy platens over which are stretched metallized mylar. With a slight tension, the flatness and reflectivity are good. The unconstrained sides of the mylar are protected by a wind guard and the entire mirror is held flat by an electrostatic hold-down.

The lightweight fiberglass can be supported and steered by an inexpensive heliostat control. To eliminate dependence on good bearings, the angle of reflected light from each mirror is sensed by a pair of 4-photocell pickups. These control the mirror to hold the reflected light aimed at the window irrespective of wind forces. The accuracy of this steering control is mainly a function of the quality and rigidity of the sensor, and is independent of motors and bearings.

SENSORS AND CONTROL

A pair of 4-quadrant light-ray angle sensors is used, with a 10-centimeter horizontal spacing between them, so that a support shadow falling on one sensor would not also fall on the other sensor. An error-correcting logic code is used so that the command signals to the tracking motors comes from the unshadowed sensor. Also, this system is fail-safe if any one photocell is nonfunctioning.

A small digital micro-computer is installed at each mirror. It controls the following mirror modes: (1) tracking an invisible sun, (2) tracking a visible sun, (3) stowed for sandstorm protection, (4) adjustment position stowing all other mirrors in a field, and (5) vertical maintenance position. This computer is automatically self-calibrating with experience in mode (2) to obtain the coordinate transformation needed for mode (1) tracking without sunshine.

PROTECTION

Temperature and flow sensors are provided for the fluids and the surfaces at each tower. In the event of an accident, compressed air can expel the TEG from the windows, immediately reducing the light transmitted by 12 percent, and the continued flow of this air can quickly cool the windows.

Commands from the sensors to the mirror computers will stow the mirrors in two minutes. An insulating shield is movable to cover the window to protect it in the event of a sandstorm and to conserve heat at night.

HEAT EXCHANGERS

The counterflow heat exchangers to evaporate the boiler feedwater, superheat and reheat the steam are cylinders approximately 3.4 meters in diameter by 15 meters tall, with coils of 1" diameter tubing containing the high-pressure steam. 6.20 meters-squared of surface area is required for each thermal megawatt. The heat exchanger shell is not a pressure vessel. The heat exchanger is surrounded by an artificial geothermal reservoir to store heat for nighttime operation, and the pressure containment vessel is around the reservoir.

ENERGY STORAGE

On the average, 30% of the heat energy received during the day is pumped into "pebble-bed" heat storage reservoirs. These are tanks full of spherical rock balls through which the hot pressurized heat-exchange fluid flows in the spaces between the balls. They heat up during the daytime. At night, the flow is reversed, and the rocks deliver to the heat-exchange fluid enough heat to keep the power plant operating at 87% power for a maximum of 5.2 hours.

THERMAL TRANSIENTS

The heat exchanger flows are controlled by the steam conditions. The solar field flows are controlled by the fluids from the receptors. When the solar energy fluctuates due to clouds passing, the rate of input of heat to the receptor fluctuates. The temperatures will be held relatively constant by controlling the flow rates of the heat exchange fluids, so that the rate of heat flow into the geothermal pebble heat reservoir will fluctuate, but the turbine temperatures and generator operation will be constant and be decoupled from the solar variations.

The same flow controls will be commanded by a central computer that continuously optimizes the performance of the power plant, maximizing the megawatt-hours of electrical generation.

FIELD PATTERN

Figure 1 shows an elevation view of the solar towers. One tower and the associated mirrors are called a module. The field of mirrors that concentrate solar light on one receptor lies to the north of the receptor. The farthest mirror reflects light at a 27° elevation angle, and the nearest mirror reflects light at a 63° elevation angle. The vertical angle of acceptance is only 36°. Only 2 mirror designs are used to minimize production costs. Figure 2 shows a view of the array of towers looking north. Each module field has a hexagon shape. The towers are guyed to minimize cost.

Figure 3 shows the plan view of the hexagons. The maximum angular deviation from the normal to the receptor window of the reflected light from the edge of the hexagon is 29.5°. A wider angle will increase the

number of mirrors per module, and the radiation power per tower. An excessive angle will increase the cosine loss, the tracking loss, and the specular reflection loss at the window. The optimum angle for minimum cost will be determined by an optimization computer program.

RECEPTOR

Figure 4 is a vertical cross-section of the heat receptor. The window is 2.1 meters wide by 2.4 meters height. The low-iron glass is coated with magnesium fluoride only at the exterior air-glass interfaces. The interpane space is filled with triethylene glycol. The fluid-glass interfaces have negligible reflection because of the high refractive index of triethylene glycol. The fluid pumping rate is controlled to hold the outlet temperature at 200°C. This performs a triple function: The fluid provides valuable heat to the steam preheaters; it keeps the windows cool for extended life; and it greatly reduces the infrared and convection losses to the environment because of the low temperature of the glass.

Most of the solar energy passes through the window and is absorbed on the coated tubes. The panel of tubes at the back is the main absorber. The smaller tubes in front form a screen which is optically equivalent to plates parallel to the incoming light. They intercept only about 30% of the incoming light. The visible light reflection from the smaller front tubes is a major loss component and is kept low by the geometry. Visible light reflected from the back panel is mostly absorbed by other tubes, but is also kept low by a high absorption coating.

The infrared radiated from the back panel is mostly absorbed by the front tubes. The infrared radiated by the front tubes is absorbed by the glass window, but is also kept low by low tube temperature and by a low emissivity coating for infrared on the front tubes. This minimizes the heat transfer to the window. In addition, there is a convection heat flow to the window. If the triethylene glycol were stagnant, the equilibrium temperature would rise to approximately 290°C, and a temperature sensor at the TEG exit would release purging air. When the window interpane space is filled with air, the solar transmission changes by $(0.96)^4 = 0.85$, which is a 15% reduction in heat to the cavity.

The heat exchange fluid is preferably dry steam at 575 pounds per square inch. It leaves the power house at approximately 340°C. At each tower, it flows successively through the front tubes, then the intermediate tubes, and lastly through the back panel, returning to the power house at 560°C.

The dimensions of the design in Figure 4 should also be optimized by computer optimization. Higher steam temperatures increase turbine efficiency. Smaller tubes save tubing costs. But both of these cost reductions require more pumping power. At the optimum temperature, the incremental electrical output with temperature rise equals the incremental pumping power loss. At the optimum tube size, the incremental cost saving with tube reduction equals the incremental cost of increased pump power.

Figure 5 shows an east-side elevation view of the mirror mounting. The elevation control can rotate the balanced mirror around a horizontal axis. In the maintenance position, the mirror surface is vertical. To protect against dust and dew, the surface can be turned down. During a sandstorm, the surface can be turned up away from the higher density sand near the ground. The pedestal height was chosen to provide a margin of clearance above the ground sand. Azimuthal rotation occurs around the vertical axis through the pedestal.

The control for both azimuth and elevation is obtained from a redundant pair of sensors mounted in-line between each mirror and the receptor, on a tripod base. The clearance in Figures 5 and 6 must be sufficient for azimuthal rotation of 120 degrees in the stow position, and 360 degrees in the maintenance position. Figure 6 is a more detailed elevation view showing the azimuth drive motor mounted on the pedestal. The mirror platen which holds the mirror film has a wind guard along the bottom edge and top edge, and slots at the east and west ends, through which the mirror film passes and is held at a slight tension to provide good specular reflectivity. The mirror structure is balanced about the vertical axis to minimize bearing friction.

Figure 7 is a detailed plan view to the same scale as Figure 6. The elevation drive motor is carried on the rotating structure and drives the mirror platen through a worm gear. The mirror platen is molded in three sections, which can each be either flat or paraboloid. In either case, the mirror film is threaded under two hold-down wires between the sections, which hold the film in contact with the platen before the electrostatic hold-down is energized.

SENSORS

The three legs of the tripod structure for the sensors in Figure 7 are supported close to three pedestal foundations.

The precision of control is a function only of the sensor sensitivity and the support rigidity. One advantage of the small module size is less tracking accuracy required than for large modules and tall towers. The sensors are located to intercept light from the bottom 2 centimeters of the mirror at midsummer noon. This minimizes the shadowing due to the supports.

Each sensor is a hollow black shadow tube with 4 photo-receptors in a ring around the base. When light from the mirror is not accurately aligned with the axis of the shadow tube, one or more of the photo-receptors is shaded. The differential voltage produced by the horizontal unbalance drives the azimuth motor, and the differential voltage produced by the vertical unbalance drives the elevation motor. Two sensors are used so that when one is shaded, the photo-receptors with the largest signals take control in an error-correcting logic circuit.

PLATEN

Figure 8 is a detail of the wind guard at the upper and lower edges of the mirror platen.

Figure 9 shows the three panels into which the platen is divided. In the simplest construction, these panels are flat, and are not designed to focus the light. The cone of the reflected light from each panel, including the angle due to the sun diameter, is small enough to pass through the receptor window.

Consequently, these panels concentrate the light, even though they do not focus it. There is an angle α (alpha) between the plane of an end panel and the center panel in Figure 9. When this angle is 0.22 degrees, the reflected cones from the three panels are coincident at 61 meters distance. When this angle α (alpha) is only 0.18 degrees, the reflected cones are coincident at 72 meters distance. Many different angles α (alpha) could be used, but to minimize production costs and manufacturing jigs, only 2 angles have been considered in this design. If paraboloid surfaces instead of flat surfaces were used, the depression at the center of each panel would only be about one millimeter. Plastic film will easily stretch to accommodate to the shape of the platen for these small deflections. Probably for a subsequent design, four paraboloid mirror platens should be considered, for slant distances respectively of 45, 55, 65, and 75 meters.

Figure 10 is an analysis of the horizontal beam width for the panel in Figure 9. The theoretical minimum beam width for focused light is the bottom dotted line. Using design A for less than 64 meters slant distance, and design B for greater slant distances, the mirrors in the center of the field straight north of the tower would produce the horizontal beam widths given by the lowest solid line. The mirrors at the edges of the field would produce beam widths given by the solid line immediately above.

When tracking errors of ± 0.25 degrees are considered for each mirror at the edge of the field, the window width required for no loss of light at the window is the highest graph in Figure 10. This is approximately 2.1 meters width, and this is the window width selected for this design.

Figure 11 is the loss factor from a statistical analysis of gaussian random angular errors in both elevation and azimuth for every mirror in the field, for a window of 2.1 meters width and 2.4 meters height. The reflecting convection shields shown in Figure 4 had the same dimensions as the window. They conserved some of the light when the angle errors were large. The main result of this analysis is that when the gaussian tracking error standard deviation (root-mean-square deviation) is less than 3 milliradians, the loss of light is negligible, but if it is 5.7 milliradians, there is a 2 percent loss of light.

STAGGER PLAN

Figure 12 is a plan view of the areas swept out by the corners of the mirrors during rotation. It can be seen that this stagger plan permits 360-degree rotation in the maintenance position of any one mirror irrespective of the angles of the other mirrors. In the horizontal stow position, a mirror with maximum positive azimuth could intersect a mirror with maximum negative azimuth unless these angles were restricted by limit switches or by the microcomputer control receiving angular information from the neighboring microcomputers.

The stagger plan permits a more rigid tripod for the sensors than a rectangular plan. It minimizes blocking at the most remote mirrors. The optimum pattern for minimizing blocking is for the N-S lines through the pedestals in Figure 12 to be modified to be radii through the towers.

Figure 13 is a vertical cross-section parallel to a sun ray at 8:30 a.m. midwinter. The analysis was made for 2.9 meters between pedestals in the East-West direction, and 1.9 meters between rows in the North-South direction. For a stagger spacing of the mirrors, each mirror row casts a shadow 40% high on the mirror row to the north. For a rectangular array of mirrors, part of the shadow falls on a near mirror, shading the bottom half, and part of the shadow falls on a farther mirror, shading only the bottom 15%.

Figure 14 is a plan view for the same time as Figure 13. The top row shows the shading with stagger spacing. 31% of the area is shaded at this time. The bottom row shows the shading with a rectangular array. 22% of the area is shaded at this time with the rectangular array. Even though the stagger array has a larger shading loss, it has less blocking loss for the most distant mirrors. It also has a more favorable foundation location for the sensors. The two different arrays are equivalent at the equinox sunrise.

Figure 15 shows the air mass effect on measured direct normal insolation at Reno when the noontime peak was one kilowatt per meter squared. The air mass reduces the insolation by an additional 30% at 7:00 a.m., and by an additional 20% at 7:30 a.m. The total daily energy was 10.1 kilowatt-hours per meter squared.

A similar curve is shown in Figure 16 for midwinter. The 30% loss occurs at 7:40 a.m. and the 20% loss at 8:10 a.m. Also shown is the effect of shading with a stagger array of mirrors. The composite has a loss of 40% at 8:30 a.m. When the mirror field and power plant operate for 8.63 hours each day, the effective energy received is 7.33 kilowatt-hours per meter squared. This analysis must be carried out for all mirrors at all hours, and combined with received radiation (insolation) records, to determine the power plant capabilities.

INSOLATION

Figure 17 is a United States map with contours of average daily radiation in Langleys. (One langley is one calorie per square centimeter.) Good

locations for solar power plants are south of Albuquerque, El Paso, Phoenix, Tucson, Las Vegas, and Inyokern. The lower bar graph in Figure 18 is the same information as Figure 17, from different sources, in units of kilowatt-hours per meter squared. El Paso received 6.23 KWH/M^2 on a horizontal surface, average for 1950 through 1962. Converting this to the direct insolation on a surface perpendicular to the sun's rays, i.e., a tracking heliostat, and subdividing into monthly averages; for the same 12-year interval, yielded the bar graphs in Figure 19 for El Paso and Inyokern. The values given in Figure 19 are the peak noon rates for energy, curves like Figures 15 and 16. The yearly average for El Paso is 0.84 KW/M^2 . The minimum is July with only 0.75 KW/M^2 . The maximums are February and November with 0.89 KW/M^2 .

There are large statistical fluctuations in this insolation rate. Figure 19 illustrates these with Inyokern data for 1963. For example, in November, the noon average was 0.8, but at least one day had 1.1 KW/M^2 . This is 38 percent higher than the average, and either the power plant turbine and generator must be oversized, or a significant amount of energy must be rejected by mirror stowing, or long-time heat storage be available to utilize this excess power at night. The least fluctuation occurs in May, where the peak day is only 14% above the monthly average. One can expect approximately one day per month of noon insolation as high as 1 KW/M^2 .

Table 1 is a monthly analysis of the El Paso insolation. The first two columns are derived from an analysis similar to Figure 16. The first column is the sunrise-to-sunset average-day length L . The second column E is the effective energy hours including the reduction due to air mass and shading effects as given in Figure 16. The third column is the calculated monthly MWH per meter squared of direct insolation, assuming 1 KW/M^2 direct midday insolation. The next to the last column W is the weather factor calculated from the actual records in Figures 18 and 19. It is the bar graph of the average noon insolation in KW/M^2 for El Paso in Figure 19.

The last column in Table 1 is the expected monthly mirror received radiation in KWH/M^2 including stagger-array shading and air-mass effects and excluding warm-up and shut-down times with less than 40% power rate.

The results of this weather analysis in Table 1 will be utilized in Tables 9, 10, and 11 for calculating dispatching and annual production.

The results of this and similar analyses have also been plotted in the top bar graph of Figure 18, to provide an annual comparison between different geographical locations. In summary, the southwest has many desirable locations, and local factors will probably be decisive in plant siting.

THERMODYNAMIC CYCLE

The steam flow for the SMITH SOLAR ELECTRIC PLANT is shown in Figure 20. The first feedwater pump receives warm feedwater from a reservoir, and raises it to 200 pounds per square inch pressure for the inlet to the first preheater, which is a heat exchanger with low-pressure triethylene-glycol for the heat source. The second preheater is a condensing heat exchanger using high-pressure turbine exhaust at 500 pounds per square inch, 338°C . Both the condensate and

the output of the first heat exchanger are each raised to 2600 pounds per square inch by the main feedwater pumps.

The third heater is the boiler. This receives 560°C dry steam at 520 pounds per square inch from the solar field, and boils water at 343°C, 2200 pounds per square inch. Dry steam was used as the heat-exchange fluid because of the abundance of experience and conventional technology.

The fourth heater is the superheater. This is a dry steam to dry steam heat exchanger. The solar field provides 560°C at 520 pounds per square inch, and the high pressure turbine receives 504°C at 2000 pounds per square inch.

70% of the exhaust from the high-pressure turbine is reheated to 504°C for the low-pressure turbine. 30% of the exhaust is used in the second preheater. The exhaust also provides dry working steam for the solar field. In the day time, the reheat steam flows through the solar field.

The low-pressure turbine exhausts into a spray condenser at 1.84 pounds per square inch absolute and 50°C. Some of the warm condensate is stored in the warm feedwater reservoir. Most of the warm condensate is pumped through a heat-rejection exchanger, a cool feedwater reservoir, and the liquid spray in the condenser. The heat-rejection exchanger rejects its heat into a cool water reservoir, which can be an open pond. The time constant of this reservoir is about a week. This should be protected or shaded from solar radiation, so that it does not heat up during the day.

The reservoir is kept cool by a dry cooling tower whose effective times of operation are at night and during high wind velocity conditions. Gravity separation can be used in the reservoir so that the coolest bottom layer is used in the heat-rejection exchanger, and the high temperature water is fed into the top layer. The tower pumps from the top layer and feeds into the bottom layer. The dry cooling tower does not need a high-power fan because it is not required to reject heat during the daytime when air temperatures are high. It operates only when the air temperatures are low, or when the wind-augmented cooling effect is efficient.

For the start-up of this system, an auxiliary boiler should be provided to generate the dry steam for the solar field receptors.

In Figure 20 are shown heat storages for the triethylene-glycol, the boiler, and the superheater. These are discussed in more detail in conjunction with Figures 23 through 28 inclusive.

Figure 21 is the Mollier diagram for the steam cycle in Figure 20. Curve A is for a turbine throttle temperature of 504°C, 940°F. Because of mechanical and turbine blade inefficiencies, the HP turbine expansion line is not vertical, down to 500 PPSI, 580°F, and H of 1285 BTU per pound, but instead terminates at 500 PPSI, 640°F, and H of 1322 BTU per pound. This loss in work done is equivalent to 78% mechanical efficiency. The reheat brings curve A back up to 940°F, 500 PPSI, and H of 1491 BTU per pound. The low pressure turbine expands the steam to the saturation line at 200°F, 12 PPSI absolute, and then into the wet region to 6% moisture at 1.84 PPSI absolute. The thermodynamic efficiency of this cycle is 38.4 percent, considering the bleeds and pump powers.

Also shown in Figure 21 is curve B for a turbine throttle temperature of 538°C, 1000°F. This cycle also expands to 1.84 PPSI absolute. Considering the bleed for the second preheater, and the feedwater pump powers, this cycle has 40.3 percent thermodynamic efficiency. This increase in efficiency is at the expense of higher collector and piping temperatures, larger field heat losses or better insulation, and more expensive heat exchangers. There is an optimum turbine input temperature for minimum cost. This can be calculated using a Fletcher-Powell or second-order optimization computer program, after detailed cost calculations are available for the system components. It is estimated that curve A will result in a lower cost than curve B, and that the curve A operating conditions also given in Figure 20 on the steam flows are near to the minimum cost design.

The first five columns of Table 2 are a detailed analysis of the cycle A from Figure 21. The sixth column is the steam rate in pounds per hour for a mechanical output of 113.9 MW. The number two heater bleed steam flow B has been calculated and included. The next to the last column shows that 49.2 MW_t is received from the triethylene-glycol. The boiler receives 132.4 MW_t, and the superheater and reheater receive 114.9 MW_t of heat. The condenser rejects 65% of all of the thermal heat collected. Special attention should be given to an efficient rejection of this heat at night, at low cost, or its utilization in chemical processes.

Table 3 is the daytime electrical balance for a 100 MW output. The 49.2 MW received from the triethylene-glycol is 17% of the total solar field heat. The boiler receives 44.4% of the field heat, and the superheater and reheater receive 38.6% of the field heat. The dry steam pumps require a significant amount of power because the vapor is compressible. This power is converted to heat in the tubing friction and reappears at the inlet to the turbine. Unfortunately, this cycle includes the thermodynamic efficiency of the turbine, so that this power is costly. Also, the compressor pumps are a significant capital investment.

Figure 22 is a plot of the heat in BTU per pound of water versus temperature. This is the same information as curve A in Figure 21. It displays graphically the heat input requirements. The characteristics of the window in the receptor can be plotted on these coordinates for different TEG pumping rates. The design point is 17% heat at 190°C. For lower pumping rates and higher window temperatures, less heat is transferred from the tubes to the window, and more heat is radiated to the environment. When the TEG is about 245°C, there is only 10% heat available from it. At the optimum design point, all of the TEG heat is usable at the available temperature. It is proposed that the TEG pumping rate should be controlled by a feedback regulator loop holding the maximum temperature at 200°C. An increase in temperature will increase the pumping rate.

HEAT STORAGE

The design of pressurized heat storage reservoirs is shown in Figure 23. The structure is prestressed concrete with a steel liner. The reservoirs operate at the pressure of the dry steam returning from the solar field. One is allocated to boiler operation and the other to superheat. The boiler itself

is inside of the pressurized vessel. Steam from the solar field passes through the boiler with loss of both temperature and pressure. The first compressor pump controls the heat exchanger flow from the sensed outlet steam condition. Increased temperature reduces the flow. The second compressor pump controls the field flow from the sensed temperature of steam returning from the field. Increased temperature increases the flow. The second compressor pumps at a higher rate than the first compressor during the daytime. The difference between these flows passes into the top of the "pebble-bed" storage and out at the bottom. The "pebble-bed" is 5-centimeter diameter granite balls with no "fines." These are heated during the day up to 530°C at the top and 460°C at the bottom, with an average temperature of 495°C.

At night, the second compressor pump is turned off, so that the heat-exchanger boiler is provided with dry steam from the heat reservoir. After several hours, the temperature drops to "depleted" values of 345°C at the top, 305°C at the bottom, and average value of 325°C at the end of the turbine operation from storage. There is a temperature cycling each day of 170°C.

The heat storage medium should be inexpensive and durable. Rock or ceramic balls are suitable if they will not crack or spall with this repeated temperature cycling. A small diameter has the advantage that it is stronger and has a smaller thermal time constant, but the pumping power requirement is larger. Engineering tests are needed to determine the minimum cost material and dimensions.

The superheater in Figure 23 receives heat from the field steam at 560°C and exhausts to a first compressor pump controlled by the HP turbine throttle temperature. Increased temperature decreases the flow. The field steam also enters the top of the heat reservoir and exhausts at the bottom. The second compressor pump receives flow from both the bottom of the heat reservoir and the bottom of the superheater, and pumps both back to the solar field. It is controlled by the returning steam from the solar field. Increased steam temperature increases the pumping rate.

The temperature gradient through the heat storage reservoir is 540°C at the top and 500°C at the bottom. Since the low pressure turbine is designed for 504°C steam, a tap is provided in the reservoir to extract 504°C steam during the fully-charged afternoon condition. This is the lowest tap shown in Figure 23.

At night, the field pump is off, and the heat-exchanger pump circulates steam through the reservoir. After several hours, the temperature range drops to the "depleted" values of 470°C at the top, 325°C at the bottom, and 400°C average. To obtain 450°C steam for the LP turbine, the "upper" tap is provided in the reservoir. For the intermediate operating conditions, a slotted spiral valve can be provided to control by rotation the quality of the input to the LP turbine.

The Mollier diagram for operation from heat storage is shown in Figure 24. Curve D is a repeat of the daytime curve A from Figure 21. Curve SF is operation with the heat storage full at maximum temperature. The feedwater pump and throttle pressures have been reduced to keep the electrical output below 105 MW_e.

Curve SD in Figure 24 is operation with the heat storage depleted to minimum temperatures. The throttle pressure has been reduced to 1400 pounds per square inch.

A detailed analysis of the heat balance for operation from storage when the storage is fully charged to maximum temperatures is given in Table 4. The thermodynamic efficiency is less because the pressure has been reduced, but the overall plant efficiency is higher because the field pump compressors are not in operation. Table 5 is the heat balance for depleted storage, with significantly reduced pressures and flow rates.

Table 6 summarizes the nighttime operation for the entire plant. The electrical output diminishes from 105.1 MW_e at full storage to 68.1 MW_e at depleted storage, with an average of 86.7 MW_e. Curves of the decrease in thermal heat flow rates as a function of time are shown in Figure 25.

The physical specifications of the thermal reservoirs can be summarized from the curves in Figure 25 and Table 6. This is Table 7 for sensible heat storage. Using granite balls of constant radius, 5592 metric tons are required for the boiler storage for each hour of operation from storage. Cost analyses of the operation of western power systems have shown that several hours of storage are probably economic when there is a large evening load peak. Selecting arbitrarily 6 hours of storage at 75% of 100 MW, or 450 MWH of storage as a possible economic amount, yields 29078 metric tons needed for the boiler, and 25704 metric tons needed for the superheater. The schedule of power delivered would be that in Figure 25, of an average of 82.8 MW_e for 5.2 hours, and not a constant 75 MW_e.

The triethylene glycol also stores energy in a pebble-bed, but the fluid in the bed is as important as the granite, because of its high specific heat. 6370 metric tons of granite and 1243 metric tons of triethylene glycol are needed for the storage design of Tables 4 through 7 inclusive and Figures 24 and 25.

POWER PLANT FIELD DESIGN

The area of solar field and number of mirrors required is a function of the collector system design and efficiency. Table 8 is a summary of efficiencies. For the mirror geometry in Figures 12 and 14, the mirror surface area is 36% of the land area. Each module has 312 mirrors. The radiation arriving at the core of the cavity in Figure 4 is 498 KW_t when the insolation is 1 KW/M². The heat delivered by both the triethylene-glycol and the dry steam to the power plant is 466 KW_t.

At this insolation level, the electrical output delivered to the transmission line would be 161 KW_e per tower, during the daytime. The electrical output due to stored heat and nighttime generation would be 164 KW_e per tower. The weather effect shown in Figure 19 and tabulated in Table 1 will reduce the electrical outputs as shown in Table 9. The output per tower averages 138.5 KW_e for 9.1 average effective hours per day, yielding 460.1 MWH_e per year per tower for daytime generation.

1. Economy of Mirror size is lost ($\sim 40-50 \text{ m}^2$ is optimal)
2. Will the high temperature damage the window coatings (mg. fluoride)?
3. It is not clear what the cavity convection losses will be. (I think both cases will be fairly small compared to radiation)
4. Weathering of mirrors, reflectivity of metalized mylar.
5. electrostatic hold down?
6. Energy storage thermoclined?
7. Pumping costs for gases will be very large.
8. Pressures are way too high for large vessels (storage) $\frac{PR}{t} = \frac{700 \times 150 \times 12}{t} =$
9. Costs for tower and receiver seem low
10. Mirror structure looks way too flimsy
11. 4 pipes for each tower field 2 TEGs, 2 Helium, piping ^{insulation} costs seem too low
12. Energy density/gr.

$$\frac{.7228 \text{ MWH}}{\text{m}^2}$$

13. Helium in distributed collector system is a bad choice

When 450 MWH of storage is included with a 100 MW plant, the output per tower per day has a maximum of 1.368 MWH_e in midsummer, and a minimum of 1.046 MWH_e in midwinter.

A field array of 1100 towers was chosen to be called a nominal 100 MW plant. The annual dispatching from this field array is shown in Table 10. Only at the spring equinox can the night heat storage be completely filled each day. At midsummer and midwinter, only 4.1 hours of storage power remains to be stored after dispatching 100 MW at all times when it is available. The storage can be operated at higher efficiency at night, but can only be 79% depleted. With this dispatching schedule, the annual production at 100% availability would be 508400 MWH. Because each night is available for preventive maintenance and repairs, the plant availability should be quite high. At 95% plant availability, the annual production would be 483000 MWH from 1100 towers, and 343,200 mirrors on 480 acres of land. This is summarized in Table 11.

A larger number of towers for the same size turbine-generator would probably not be economic because more heat would be received during the spring months than could be either stored or utilized, and to hold the temperatures below maximum safe values, some of the mirrors would have to be stowed some of the time. Even with this design, there can be several days of exceptionally high insolation, corresponding to the highest circled points in Figure 19, which might result in some mirrors being stowed for temperature limiting.

FUSION STORAGE

Storage costs are relatively high, and attention should be given to alternative engineering designs that have promise of reducing the cost. One method of reducing the cost of a sensible heat storage design like Figure 23 is to obtain low cost, high heat capacity, high temperature materials.

Another approach is to examine the properties of a system using heat of fusion. Figure 26 is helpful in determining the desirable properties of a heat-of-fusion storage system. One fusion pot is not sufficient and two different materials are provided, one melting at 420°C and the other melting at 510°C. The farthest left line is the turbine steam heat input requirements above 290°C (exclusive of the first two preheaters), for an electrical output of 100 MW_e and a steam inlet condition of only 470°C, 1800 PPSI. The temperature was reduced in order to have sufficient temperature differentials between the solar field steam, the fusion material, and the turbine steam. This graph is a modification of Table 4 for the cycle shown in Figure 27, and is analogous to the upper part of Figure 22 multiplied by the steam flow rates C' and A' in Table 4.

The farthest right sloping line in Figure 26 is the heat available from the dry steam in the solar field, in which all of the steam flows sequentially through first the high temperature fusion pot, and then the low temperature fusion pot. The flow rate was chosen for a temperature range from 560°C maximum to 440°C for the steam returning to the solar field. The fusion characteristic must lie between these two extremes. The 420°C pot can receive heat from the dry steam over the range of 535°C down to 440°C.

It can deliver heat to the turbine steam over the range 335°C down to 290°C. The 510°C pot can receive heat from the dry steam over the range of 560°C down to 535°C, and can deliver heat to the turbine steam over the range 470°C down to 385°C. The low temperature pot must deliver 200 MW_t while the high temperature pot must deliver only 50 MW_t.

Figure 27 is the Mollier diagram for the design chosen in Figure 26.

Figure 28 is the fusion storage system flow diagram. The material chosen for the 510°C pot was 30% Aluminum and 70% Zinc. This has 42.7 calories per gram heat of fusion. The pot is ceramic lined. The turbine tubes are nickel-plated inconel and the dry steam tubes are nickel-plated stainless. The latter have zone-melting-control valves so that the vat is melted from the top down, and freezes from the bottom up. To deliver 51 MW_t, this pot must contain 1026 metric tons for each hour of storage at 100 MW_e.

The material for the 419°C pot is zinc with 28.13 calories per gram heat of fusion. This pot is both boiler and partial superheater. It also has zone-melting control to melt from the top down. At night, when the solar field flow is zero, the dry steam pipes carry the reheat steam. This pot contains 6112 metric tons per hour of storage at 100 MW_e.

Where two temperatures are written, one above and the other below a horizontal line, these are daytime and nighttime operating conditions respectively.

The heat of fusion of aluminum is much higher than that of zinc. It would seem to be economic to store more heat in the high temperature pot, and to operate it at a higher temperature, using a greater proportion of aluminum. But Figure 26 shows that this will result in some of the dry steam being returned to the solar field at a much higher temperature, reducing its heat carrying ability per pound, and increasing the pumping cost. Increasing the turbine inlet temperature to achieve higher efficiency also moves the curves in Figure 26 to the right, and increases the pumping costs. A practical fusion-storage design will need an engineering study to select the material and system to minimize the cost per MWH of storage.

PIPING

The simplest piping system is north-south headers in Figure 2 passing by the base of each tower. There would be a low-temperature high-pressure dry steam header from the plant, a high-temperature low-pressure dry steam header back to the plant, and supply and return triethylene-glycol lines. Each tower would be in parallel across the headers. This will result in a rectangular field shape. Each piping tree length will be 54.9 kilometers.

An alternative is to align the headers diagonally through the fields passing by the base of each tower. This could yield a field shape and piping tree as shown in Figure 29. Here the tree length is only 47.8 kilometers. Comparative costs for these alternatives should be determined.

OPTIMIZATION

Computer programs are available for sophisticated cost minimization to determine design dimensions and parameters. These programs need detailed factory overhead, materials, labor, installation, construction overhead, and interest costs for a specific engineering design. A feasibility study of this design should include the detailed engineering for a 100 MW_e plant.

DESIGN CONTINGENCIES AND ALTERNATIVES

This design is intended to have high reliability at low cost. For high reliability, the system is subdivided into small units, any one or group of which can be operated independently of units which have been removed from service for maintenance or repairs. Low energy density at the heat receptor is favorable for high reliability, long life, and low cost. The unique features of this design also provide good efficiency, through reclamation of losses.

The design is not dependent upon particular special or critical components. For nearly every component there is an acceptable available alternative. An alternative for each component has been considered and will be studied.

The first mirror surface can be Sheldahl 2 mil polyester base (mylar or melanex) first surface of 700 Angstroms silver with monolamic 822 (acrylic base) covering which has a specular reflectance of 0.95 maximum.

A suitable window glass is low-iron water-white ASG Crystal #76 which is available in 7/32" nominal thickness in 1.2-meter (48") widths. It has a solar absorption of 1.5% in this thickness, primarily in the infrared. The refractive index is 1.519. The cost is approximately \$2.50 per square foot. The thermal expansion coefficient is 47×10^{-6} per degree F or 84.6×10^{-6} per degree C. The modulus of elasticity is 10.5×10^6 psi. The weight is 2.8 pounds/ft².

A suitable coolant fluid for the window is Union Carbide Triethylene Glycol. It has a refractive index of 1.456, a viscosity of 49 cps. at 20°C, a boiling point of 288°C at 760 mm pressure, and a freezing point of -4.3°C. Glass, stainless steel, silicone, and soft teflon are suitable materials for the window construction. A small amount of amine can be used in the TEG to hold the pH basic near 8. It probably decomposes at elevated temperatures above 300°C to esters and ketones. Vents to the system on the high temperature side can be used to prevent water from entering the system. Water will lower the refractive index. When the transmissivity of the TEG deteriorates due to decomposition products, it can be processed in a reclaiming system to distill off the moisture, and then in a second still save the top and throw away the bottoms.

OPERATING CONTINGENCIES

In the event that the window is removed for maintenance or repair, the heat receiver can continue to operate at the rated temperature but with reduced thermal output. The output will be reduced from 466 KW_{th} to 350 KW_{th}, a loss of 25%.

In the event that the window is cracked and the fluid is missing, there will be 65 KW removed from the core. This will require a shutdown by moving the mirrors into the stowed position as a function of either sensed lack of flow or elevated temperature at the window.

In the event that the TEG pumps fail and the fluid is stagnant in the window, there will be 79 KW absorbed in the window and the temperature will start to rise to the stagnant value of 290°C. This temperature is below but close to the temperature that would decompose the TEG. Again, sensed lack of flow or elevated temperature or positive rate of increase of temperature should be used to move the mirrors into the stowed position.

The window glass has a thermal expansion coefficient close to steel, and can be mounted in a steel frame with silicone or soft teflon seals to provide for thermal expansion and for nonuniform temperature distributions. The effect of thermal shocks will be investigated. The stresses due to the static temperature gradient across the glass and the dynamic changes when the mirrors move from stowed to concentrating must be studied.

In the event that either the glass is etched by corrosion or that the antireflective coatings deteriorate, the system can continue to operate with a slightly reduced electrical output. The windows will be removable for the replacement of the glass as a maintenance procedure if desired. The plant can be operated at reduced power without windows. If Crystal #76 is used without antireflective coatings, the power will be reduced 4%.

In the event that the main feedwater pump fails, the rise of temperatures in the heat exchange fluids should stow the mirrors.

INDEX OF TABLES

Table

1	Weather and Date Effect per Meter Squared, El Paso
2	Steam Heat Balance, Nominal Daytime
3	Electrical Balance, Daytime
4	Heat Balance, Full Storage, Night
5	Heat Balance, Depleted Storage, Night
6	Thermal Input, Nighttime, From Storage, MW
7	Sensible Heat Storage Requirements
8	Solar Power Field Module
9	Weather Effect
10	Annual Dispatching
11	100-Megawatt Generation Unit

TABLE 1
 WEATHER AND DATE EFFECT PER M², EL PASO, 31.8° N. LAT.

Date	L	E	R	W	P
January	10.4	7.5	232.5	0.88	204.6
February	11.1	8.2	229.6	0.89	204.3
March	11.9	9.0	279.0	0.86	239.9
April	12.9	10.0	300.0	0.86	258.0
May	13.8	10.9	317.9	0.83	280.5
June	14.1	11.2	336.0	0.80	268.8
July	13.9	11.0	341.0	0.75	255.8
August	13.3	10.4	322.4	0.80	257.9
September	12.4	9.5	285.0	0.82	233.7
October	11.5	8.6	266.6	0.86	229.3
November	10.7	7.8	234.0	0.89	208.3
December	10.2	7.3	226.3	0.88	<u>199.1</u>
Sum					2,840.2 KWH/M ² /YEAR
					7.781 KWH/M ² /DAY

L = Day length in hours.

E = Effective energy hours = L - 2.9 (Includes air mass and shading effects).

R = Received energy in MWH/M² at 1.0 KW/M² direct midday insolation, monthly.

W = Expected weather factor, 12-year average.

P = Expected total production, MWH/M²/MONTH. P = R · W.

Reference: Iven Bennett, Solar Energy, Vol. 9, No. 3, 1965, 145-158.

TABLE 2

STEAM HEAT BALANCE, NOMINAL DAYTIME

	P	T	T	H	ΔH	F	ΔFH	Useful Work
	$\frac{\#}{\text{IN}^2}$	°F	°C	$\frac{\text{BTU}}{\#}$		$\frac{\text{Flow \#}}{\text{Hour}}$	MW_t	MW
Feedwater	200	122	50	90.1		A		
#1 HTR from 205°C TEG	200	374	190	347.0	256.9	A	49.2	
Feedwater Pumps	2600				11.0		2.1	
#2 HTR from HP Exhaust	2600 2400	384 599	196 315	358.0 621.8	263.8	A A		50.5
HP Exhaust	500	640	338	1321.4		B		
Condensate	500	467	242	449.7	-871.7	B	- 63.0	
Reheated Cond.	2400	599	315	621.8	172.1	B	12.4	
Sum #2 Heater	2400	599	315	621.8		C	62.9	
Boiler	2200	649	343	1123.8	502.0	C	132.4	
Superheater	2000	940	504	1436.3	312.5	C	82.4	
HP Turbine	500	640	338	1321.4	-114.9	C		30.3
Bleed for #2 HTR	500	640	338	1321.4		-B		
Reheat	500	940	504	1491.3	169.9	A	32.5	
LP Turbine	1.84	122	50	1055.0	-436.3	A		83.6
Condenser	1.84	122	50	90.1	-964.9	A	-184.9	
Total Input							296.5	
Work Done								113.9
Efficiency, Thermodynamic								0.384

Flow A = 653,568 Pounds per hour
 Flow B = 246,443 Pounds per hour
 Flow C = 900,010 Pounds per hour
 # = Pounds steam

7/1-523, 57
 737
 0.384

TABLE 3

ELECTRICAL BALANCE, DAYTIME

Thermal Input to Steam		296.5 MW _t
Shaft Power		113.9 MW
Generator Losses (1.25%)	1.43 MW _e	
Electrical Generation		112.5 MW _e
Feedwater Pumps	2.3 MW	
Auxiliaries	0.5 MW	
Heat Exchanger Daytime Pumps (Dry Steam Compressors)	9.9 MW _e	
Net Daytime Electrical Output		99.8 MW _e

THERMAL INPUT, DAYTIME, FROM FIELD

TEG		49.2 MW _t
Boiler	132.4-4.2 MW (Pump)	128.2 MW _t
Superheater	82.4-2.6 MW (Pump)	79.8
Reheater	<u>32.5-1.0 MW (Pump)</u>	<u>31.5</u>
Total, Daytime	247.3-7.9	288.6 MW _t

Net Daytime Power Plant Efficiency 34.6%

TABLE 4

HEAT BALANCE, FULL STORAGE, NIGHT

	P	T	T	H	ΔH	F	ΔFH	Useful Work
	$\frac{\#}{\text{IN}^2}$	$^{\circ}\text{F}$	$^{\circ}\text{C}$	$\frac{\text{BTU}}{\#}$		$\frac{\text{Flow}}{\text{Hour}}$	MW_t	MW
Feedwater	200	122	50	90.1		A'		
#1 Heater	200	374	190	347.0	256.9	A'	49.2	
Pumps	2310				9.8		1.9	
#2 HTR	2310	383	195	356.8				
	2140	511	266	503.0	146.2	A'	28.0	
HP Exhaust	520	670	354	1337.8				
Condensate	520	471	244	454.4	-883.4	B'	- 29.6	
Reheated Cond.	2140	511	266	503.0	48.6	B'	1.6	
Sum #2 HTR	2140	511	266	503.0		C'	29.6	
Boiler	1970	633	334	1141.0	638.0	C'	143.6	
Superheater	1800	940	504	1457.0	316.0	C'	71.1	
HP Turbine	520	670	354	1337.8	-119.2	C'		26.84
Bleed for #2 HTR	520	670	354	1337.8		-B'		
Reheat	500	940	504	1491.3	153.5	A'	29.4	
LP Turbine	1.8	122	50	1055	-436.3	A'		83.59
Condenser	1.8	122	50	90.1	-964.9	A'	-184.9	
Total Input							293.3	
Work Done								110.43
Efficiency								0.3765

A' = 653,568 Pounds per hour

B' = 114,440 Pounds per hour

C' = 768,008 Pounds per hour

= Pounds Steam

TABLE 5

HEAT BALANCE, DEPLETED STORAGE, NIGHT

Feedwater	200	122	50	90.1		A''	
#1 HTR	200	176	80	144.0	53.9	A''	13.7
Pumps	1850				7.8	A''	1.5
#2 HTR	1850	184	84	151.8			
	1700	513	267	505.5	353.7	A''	44.6
HP Exhaust	350	530	277	1269.1		B''	
Condensate	350	432	222	409.8	-859.3	B''	- 50.2
Reheated Cond.	1700	513	267	505.5	95.7	B''	5.6
Sum #2 HTR	1700	513	267	505.5		C''	50.2
Boiler	1550	600	316	1165.2	659.7	C''	121.8
Superheater	1400	840	449	1399.5	234.3	C''	43.3
HP Turbine	350	530	277	1269.1	-130.4	C''	24.1
Bleed for #2 HTR	350	530	277	1269.1		-B''	
Reheat	330	840	449	1442.0	172.9	A''	21.8
LP Turbine	1.84	122	50	1055.0	-387.0	A''	48.84
Condenser	1.84	122	50	90.1	-964.9	A''	-121.8
Total Input							200.6
Work Done							72.9
Efficiency							0.364

A'' = 430,552 Pounds per hour

B'' = 199,455 Pounds per hour

C'' = 630,007 Pounds per hour

= Pounds steam

TABLE 6

THERMAL INPUT, NIGHTTIME, FROM STORAGE, MW

	Storage Full	Average	Depleted Storage
TEG #1 HTR	49.2	31.5	13.7
Boiler	143.6	132.7	121.8
Superheater and Reheater	100.5	82.8	65.1
Feedwater Pump	<u>1.9</u>	<u>1.7</u>	<u>1.5</u>
Total Thermal Input to Steam	295.2	248.7	202.1
Shaft Power	110.4	91.7	72.9
Generator Losses	1.4	1.1	0.9
Electrical Generation	109.0	90.6	72.0
Feedwater Pumps	2.1	1.9	1.7
Auxiliaries	0.5	0.5	0.5
Heat Exchanger Pumps	0.8	1.0	1.2
Cooling Tower Fan	0.5	0.5	0.5
Net Electrical Output	105.1	86.7	68.1
Efficiency	0.358	0.351	0.34

TABLE 7

SENSIBLE HEAT STORAGE

	Average Temperature Change, °C	Average Power MW	Volume of Heat Storage $\frac{\text{M}^3}{\text{StorageHour}}$	Mass of Granite Balls $\frac{\text{Tons}}{\text{StorageHour}}$	For 450 MWH Storage (5.2 Hours at 86.7 MW Mass Tons
Boiler	170	132.7	3196	5592	29078
Superheater and Reheater	120	82.8	2825	4943	25704
TEG Storage	90	31.5	700	1225	6370
Liquid TEG				239	1243
Volume Specific Heat of Balls,		0.21			
Density, Granite Balls,		1.75			
Specific Heat, TEG, Average.		0.64			
Density, TEG,		1.026			

TABLE 8

SOLAR POWER FIELD MODULE

LAND UTILIZATION, EACH MODULE

North-South	Mirror Spacing	1.90 Meters	52.6% Utilization
East-West	Mirror Spacing	2.90 Meters	69.0
Composite			36.3

312 Mirrors in 1725 M^2 with 624 M^2 Reflecting Surface

EFFICIENCY FOR ONE MODULE

ASSUMING INSOLATION AT 72% TRANSMISSION

		1.00 KW/M^2
Incident Insolation Per Tower (per module)		624.0 KW
Tower Shadow Effect	(0.994)	620.0 KW
Mirror Reflection Factor	0.91	
Composite Cosine Factor for 10 hour Day	0.92	
Tracking Accuracy	1.00	
Window Solar Reflection Factor	0.96	

Radiation Arriving at Core of Cavity 498.0 KW

Core Reflection Loss (effective emissivity)	0.997	
Thermal Watts Received		497.0 KW
IR Radiation Loss from Window*	4.75 KW	
Convection Loss (9MPH wind)	7.77 KW	
Insulation Loss	15.00 KW	
Heat Storage	.992	
Thermal Input to Turbine, Average		466.0 KW_t

TURBINE AND GENERATOR EFFICIENCY

Daytime Efficiency T-G	.379	
Plant Efficiency, Day		.346
Electrical Output per Tower at $1 \text{ KW}/\text{M}^2$		161 KW_e
Nighttime Efficiency, T-G	.367	
Plant Efficiency, Night		.351
Electrical Output per Tower Through Storage at $1 \text{ KW}/\text{M}^2$		164 KW_e

* At maximum temperature with storage fully charged. The average loss is less.

TABLE 9

WEATHER EFFECT

1.0 KW/M ² Midday Normal Insolation Yields	9.1 KWH _t /M ² /Day
	3.32 MWH _t /M ² /Year
	3322 Effective Hours/Year
 El Paso Records Are Equivalent to Insolation	
	0.86 KW/M ²
	7.78 KWH _t /M ² /Day
	2.84 MWH _t /M ² /Year
	3322 Effective Hours/Year
 Electrical Output Per Tower	
Direct Flow	138.5 KW _e for 3322 Hours
	460.1 MWH _e /Year
	1.26 MWH _e /Day
Through Storage	140.7 KW _e for 3322 Hours
	467.3 MWH _e /Year
	1.28 MWH _e /Day
 Because of Limited Storage	
Direct Flow	70% of Annual Energy
Through Storage	30% of Annual Energy
Composite per Tower	462.3 MWH _e /Year
Annual Average	1.266MWH _e /Day/Tower
Spring Equinox	1.297MWH _e /Day/Tower
Midsummer	1.368MWH _e /Day/Tower
Fall Equinox	1.235MWH _e /Day/Tower
Midwinter	1.046MWH _e /Day/Tower

TABLE 10

ANNUAL DISPATCHING

Insolation, El Paso Records			Operating Time
Average	7.78	$\text{KWH}_t/\text{Day}/\text{M}^2$ of Mirror	(9.5 hrs/day)
Spring Equinox	7.97		(9.5 hrs/day)
Fall Equinox	7.59		(9.5 hrs/day)
Midsummer	8.41		(11.5 hrs/day)
Midwinter	6.43		(7.5 hrs/day)

Electrical Output

Average	1266	$\text{KWH}_e/\text{Day}/\text{Tower}$
Spring Equinox	1297	
Fall Equinox	1235	
Midsummer	1368	
Midwinter	1046	

ENTIRE POWER PLANT OF 1100 TOWERS

	<u>Day Load</u>		<u>Night Load</u>		<u>Daily Output</u>
	MW_e	Hrs	MW_e	Hrs	MWH_e
Spring Equinox	103	9.5	87	5.2	1427
Midsummer	100	11.5	87	4.1	1505
Fall Equinox	100	9.5	87	4.7	1359
Midwinter	100	7.5	87	4.1	1151

Annual Output, Maximum	508,430 MWH_e
At 95% Availability	483,008 MWH_e

TABLE 11

100-MEGAWATT GENERATION UNIT

Number of Towers and Modules per Generator	1,100	
Land Area of Heliostats	427 Acres	1.90 KM ²
Additional Area for Cooling Tower and Plant	30 Acres	
Roads	<u>27 Acres</u>	
TOTAL LAND	484 Acres	
Number of Mirrors Required	343,200	
Plant Rating	100 MW _e	
Effective Annual Hours at Plant Rating	5,084 Hours	
Actual Annual Hours	5,119 Hours	
Annual Production (100% Availability)	508,430 MWH _e	
Annual Production (95% Availability)	483,008	

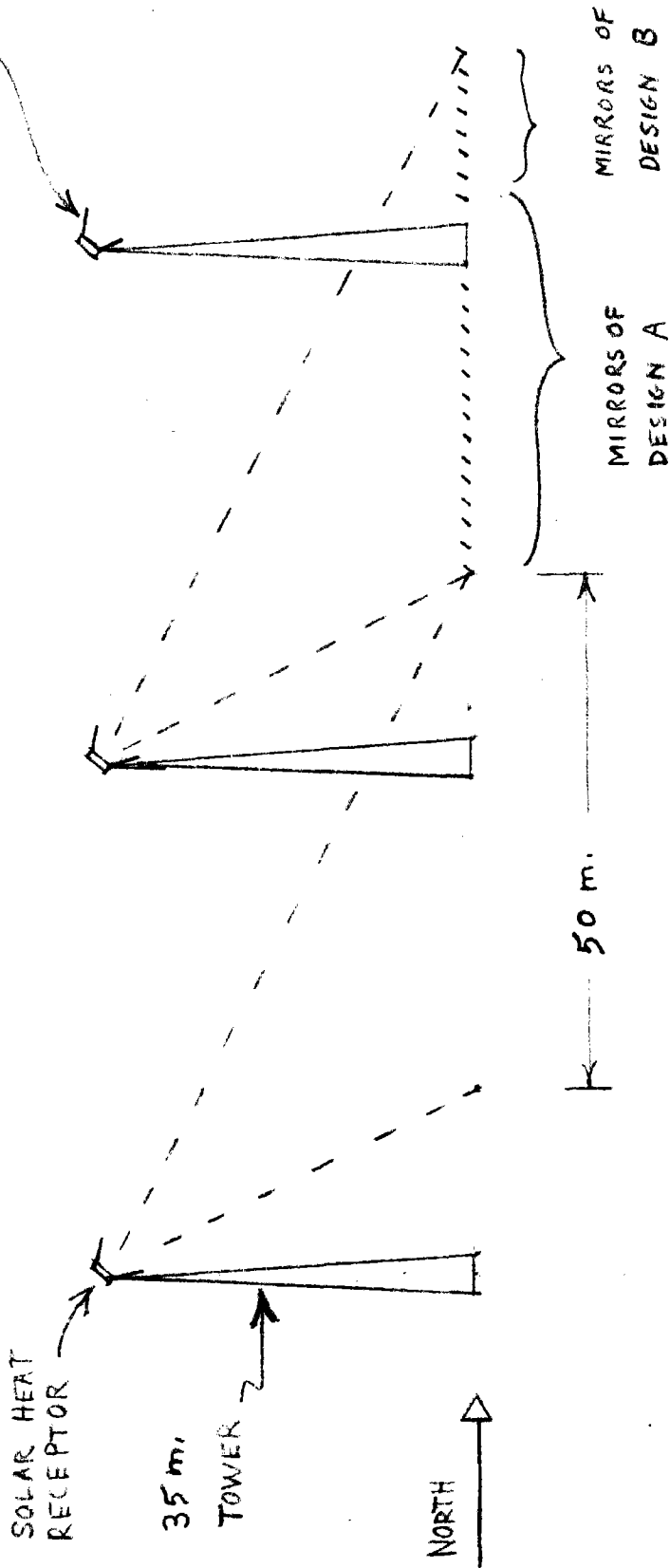
INDEX OF FIGURES

1. Elevation View of Solar Towers
2. Solar Fields Looking North
3. Plan View of Hexagonal Field Modules
4. Smith Solar Energy Receptor
5. East Side View Mirror Mount
6. Mirror Mount East Side View
7. Mirror Mount Plan View
8. Detail of Wind Guard
9. Mirror Panel
10. Window Width Required for $\pm 0.25^\circ$ Tracking Error
11. Composite Loss Factor for Gaussian Random Distribution of Angle Errors
12. Extreme Radii Rotations of Heliostat Mirrors
13. Midwinter Sunrise, Elevation View Looking Southwest
14. Plan View of Mirrors, Midwinter Sunrise
15. Measured Direct Normal Insolation, Reno
16. Shading Effect on Direct Normal Insolation, Midwinter Sunrise
17. Mean Daily Solar Radiation, Annual
18. Mean Direct Normal Insolation, Computed
19. Direct Normal Midday Insolation Monthly Averages
20. Smith Solar Electric Plant; Day Steam Cycle
21. Mollier Diagram of Steam System, Comparison of 504°C Maximum and 538°C Maximum
22. H_2O Heat of Fluid, Daytime Operation
23. Pressurized Heat Storage Reservoir
24. Mollier Diagram of Steam System. Storage Full and Depleted.
25. Sensible Heat Storage Requirements

INDEX OF FIGURES (continued)

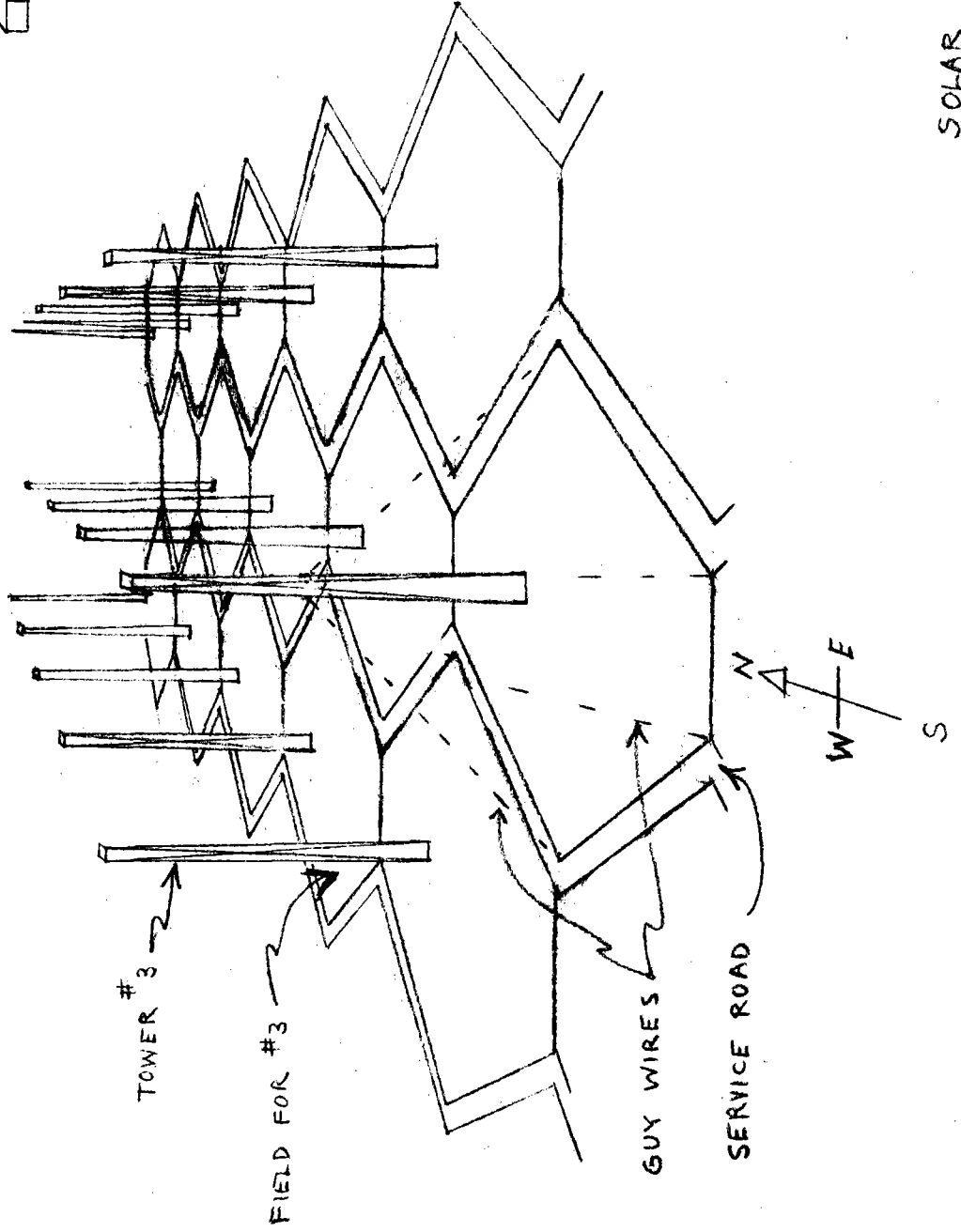
- 26. Fusion Storage Characteristics
- 27. Steam Cycle for Operation from Fusion Storage
- 28. Fusion Storage System
- 29. Piping Tree

REFLECTING CONVECTION SHIELDS
AND SANDSTORM SHUTTERS



ELEVATION VIEW OF SOLAR TOWERS

DRY COOLING TOWER
HEAT EXCHANGERS AND
TURBINE - GENERATOR



SOLAR FIELDS LOOKING NORTH

FIG. 2
OJMS 12 OCT 75

PLAN VIEW OF HEXAGONAL FIELD MODULES

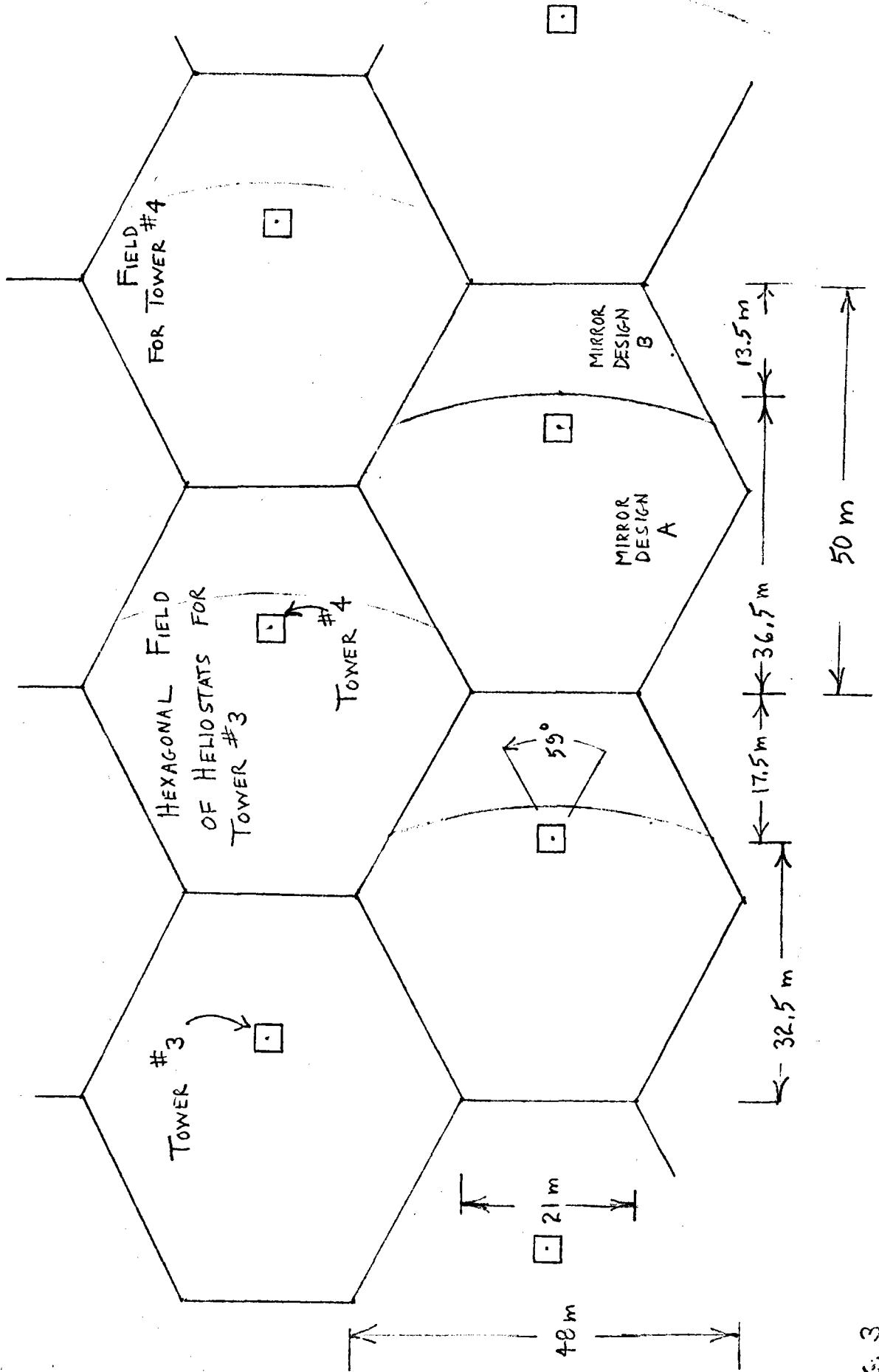
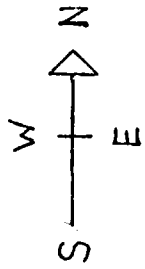


FIG. 3
OJMS 12 OCT, 75

SMITH SOLAR ENERGY RECEPTOR

2.1 meters WINDOW WIDTH

5.04 M² WINDOW AREA

TEG ≡ TRIETHYLENE GLYCOL

REFRACTIVE INDEX = 1.456

B.P. = 208°C

M.P. = -4.3°C

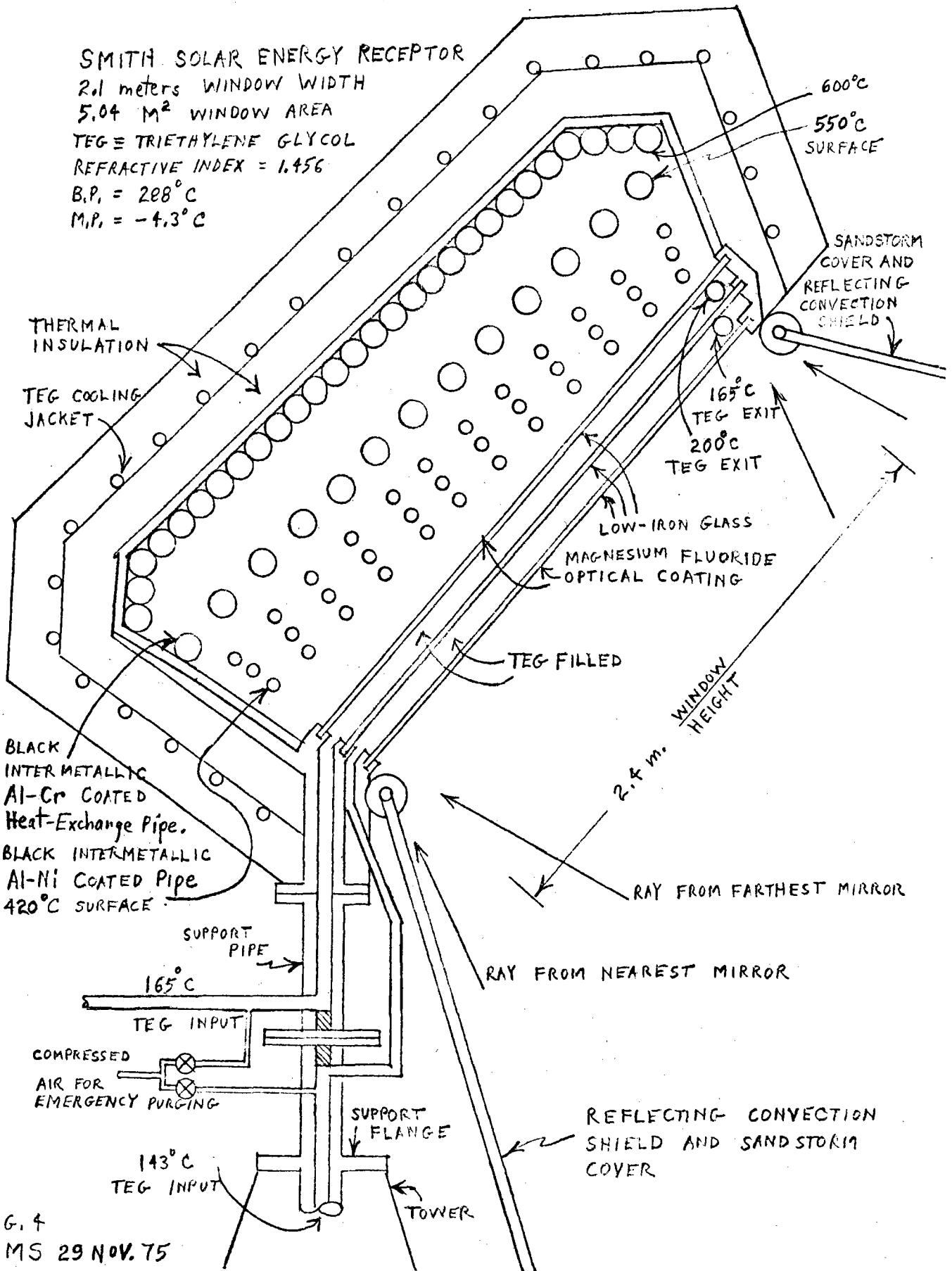


FIG. 4
OJMS 29 NOV. 75

EAST SIDE VIEW
MIRROR MOUNT

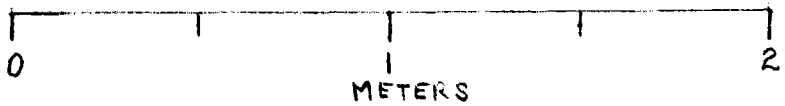
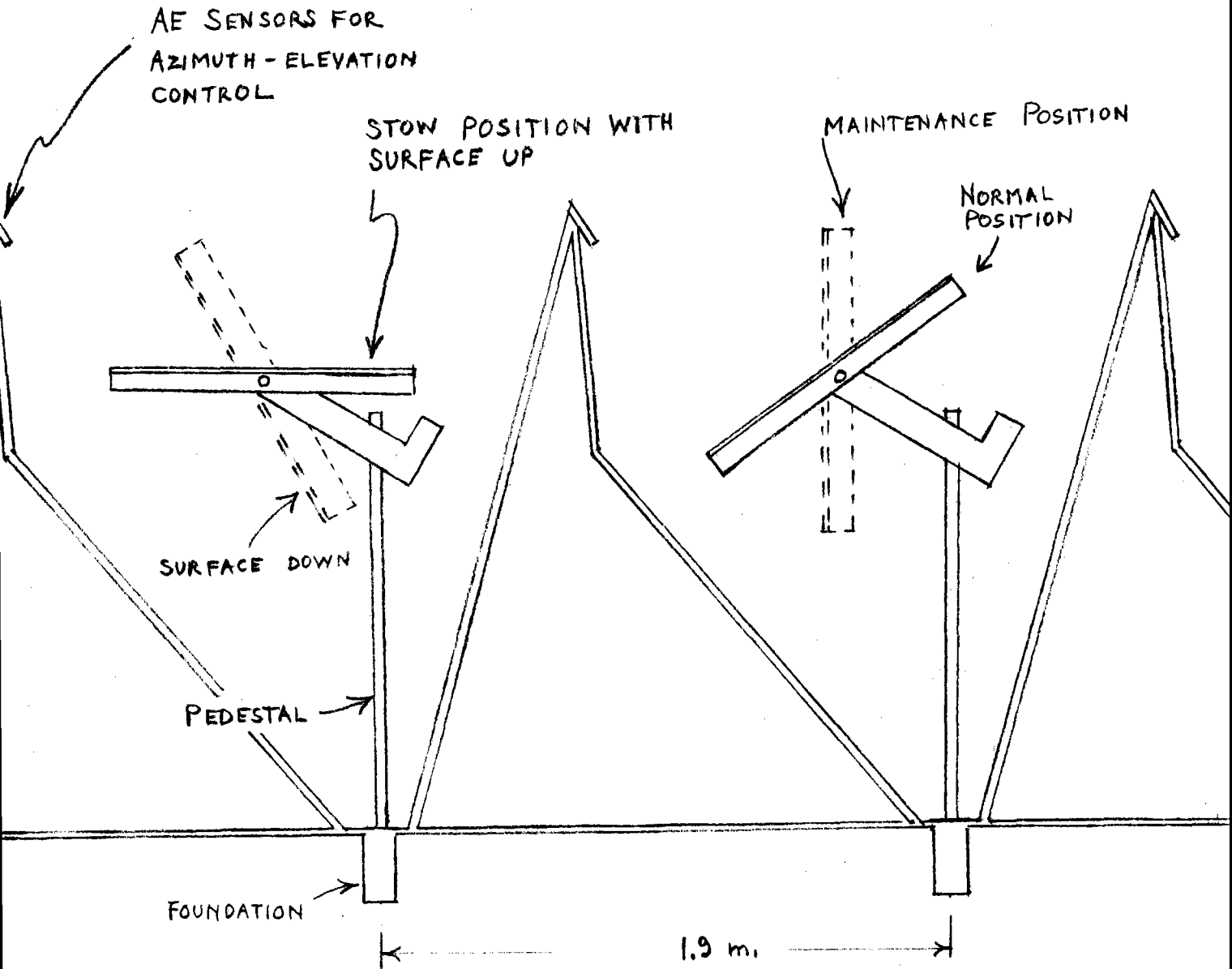


FIG. 5

D.J.M.S., 6 DEC. 75

MIRROR MOUNT EAST SIDE VIEW

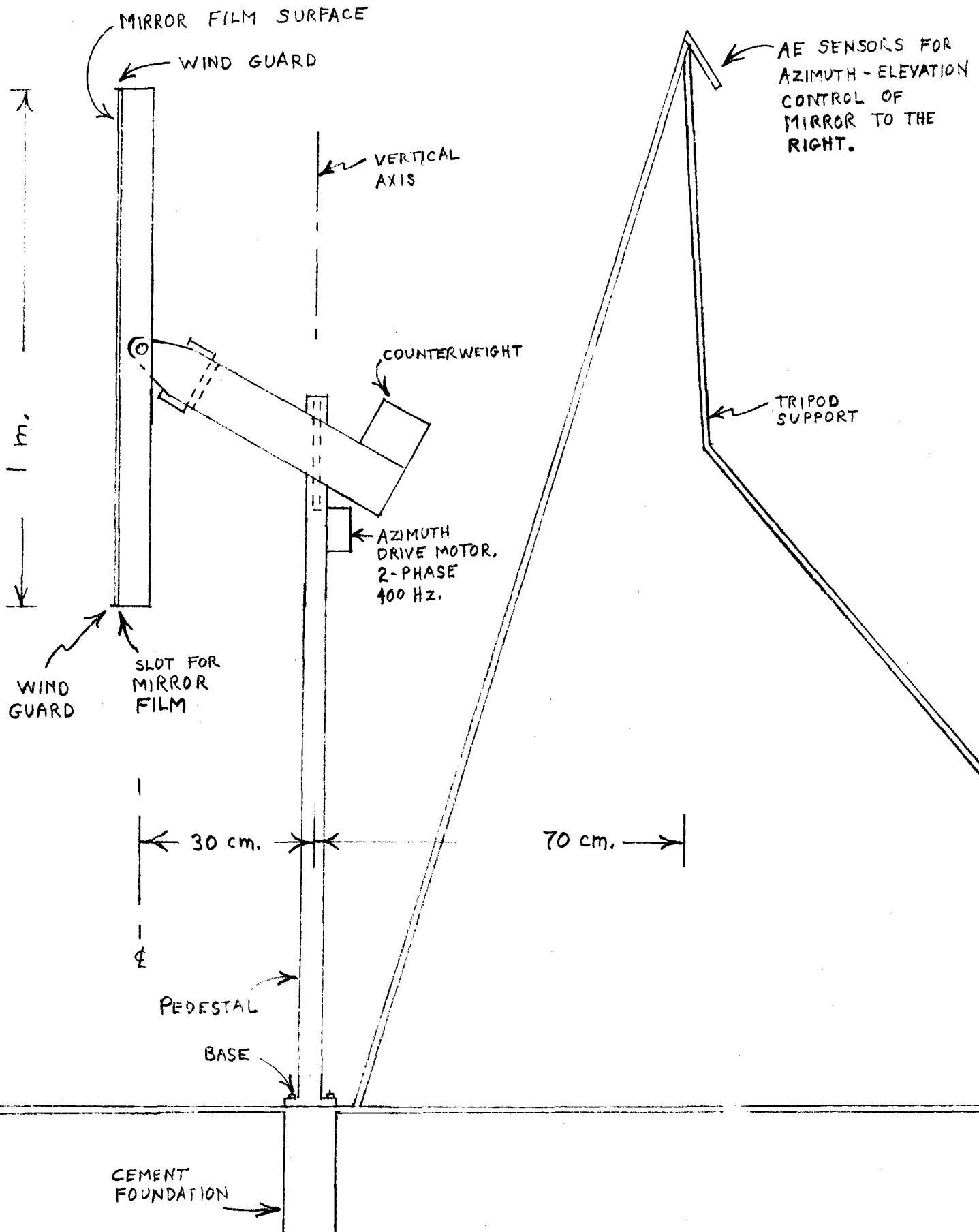
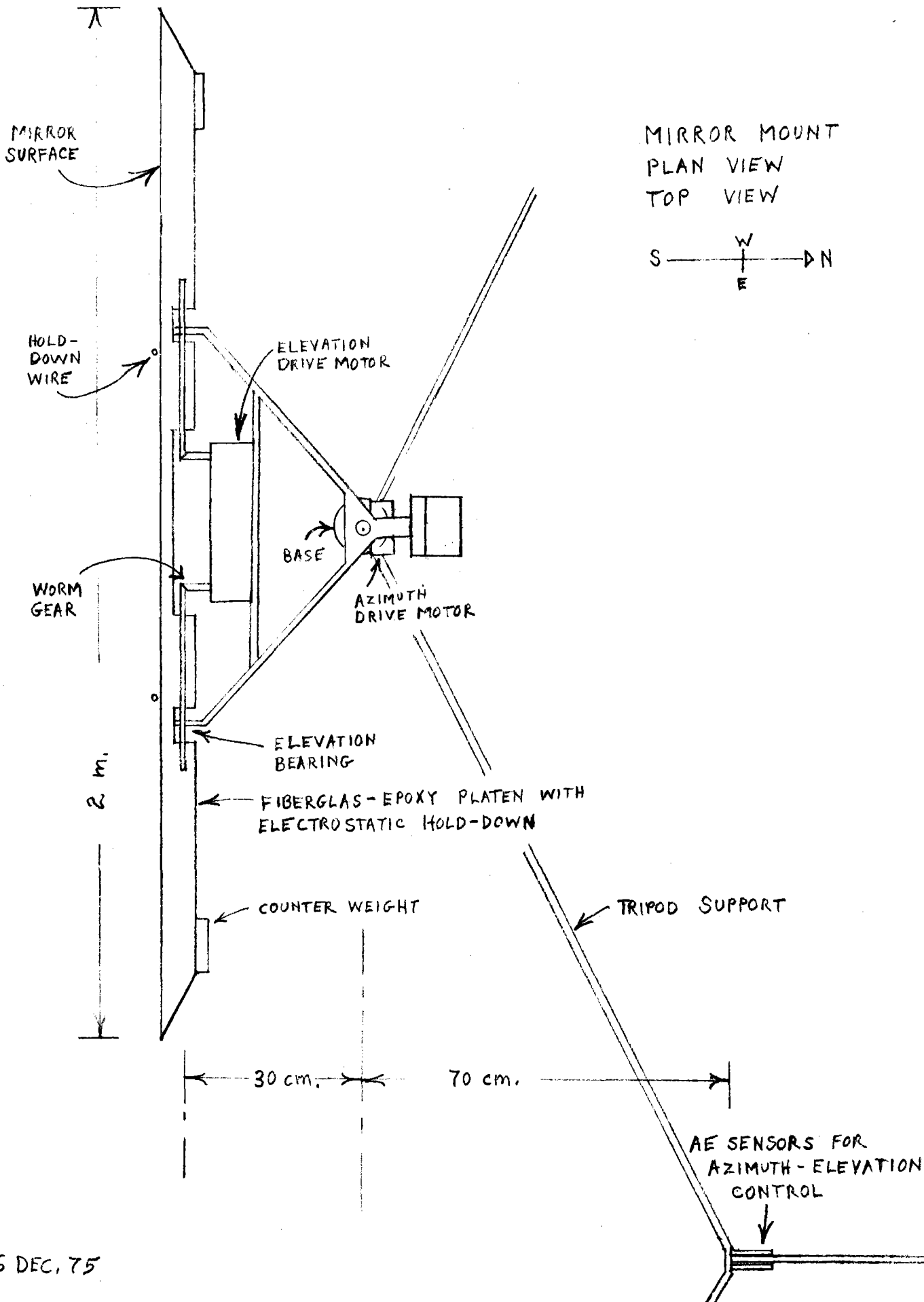
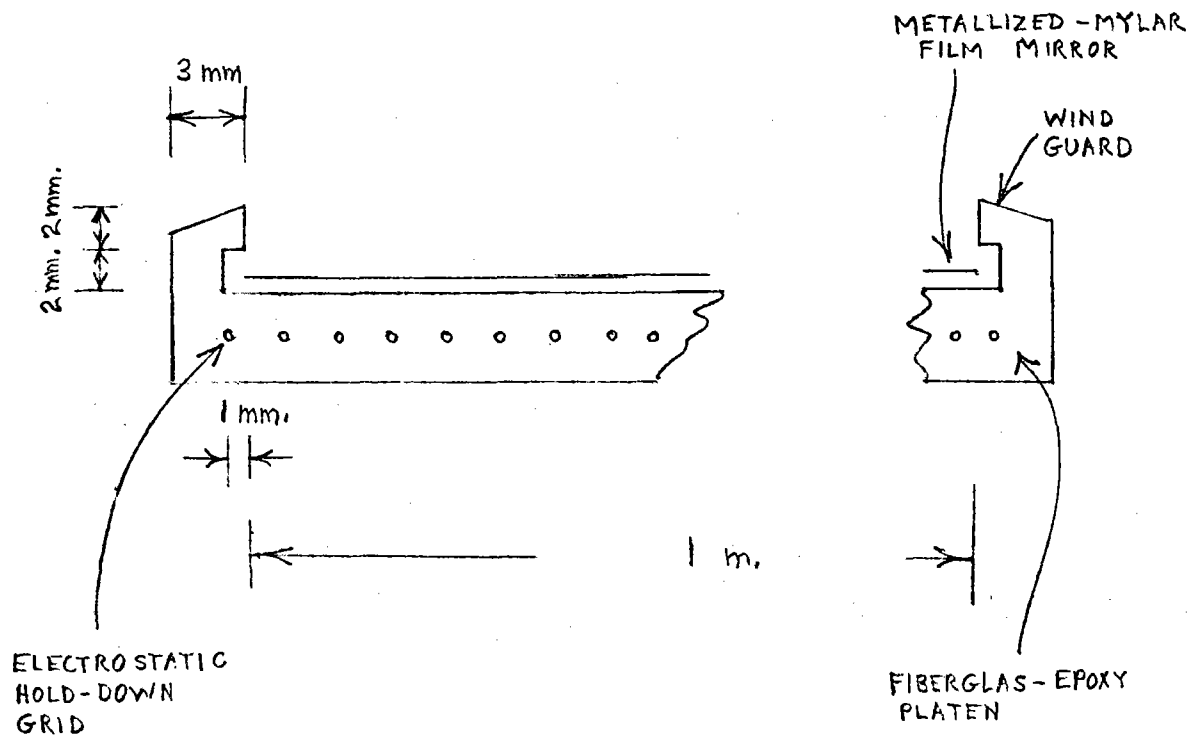


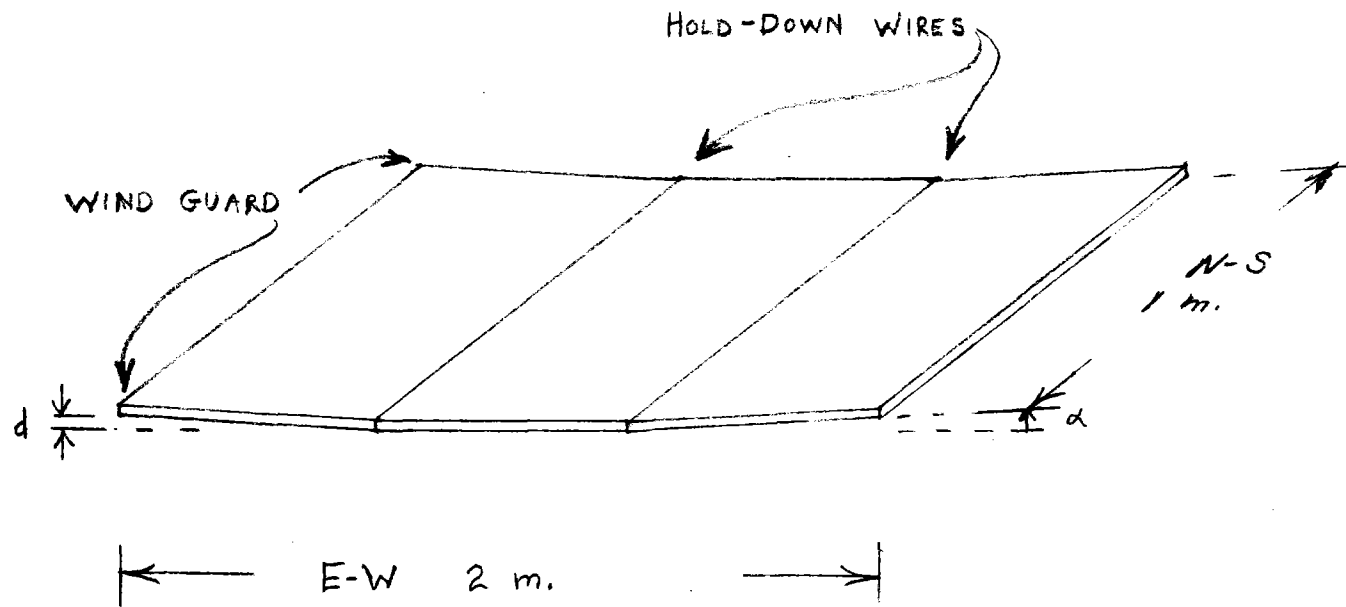
FIG. 6
J.M.S. 6 DEC. 75



F. 7
MS 6 DEC. 75

FIG. 8
DETAIL OF WIND GUARD





MIRROR PANEL

3 FLAT PANELS FOR EACH MIRROR

DEPTH OF CENTER PANEL, d

ANGLE α

MINIMUM CONCENTRATED BEAM WIDTH

HORIZONTAL DISTANCE TO MINIMUM BEAM WIDTH

USE FOR

DESIGN A

DESIGN B

2.5 mm

2.1 mm

0.22°

0.18°

1.44 m.

1.58 m.

72. m.

93. m.

< 78 m.

> 79 m.

METERS WINDOW
WIDTH

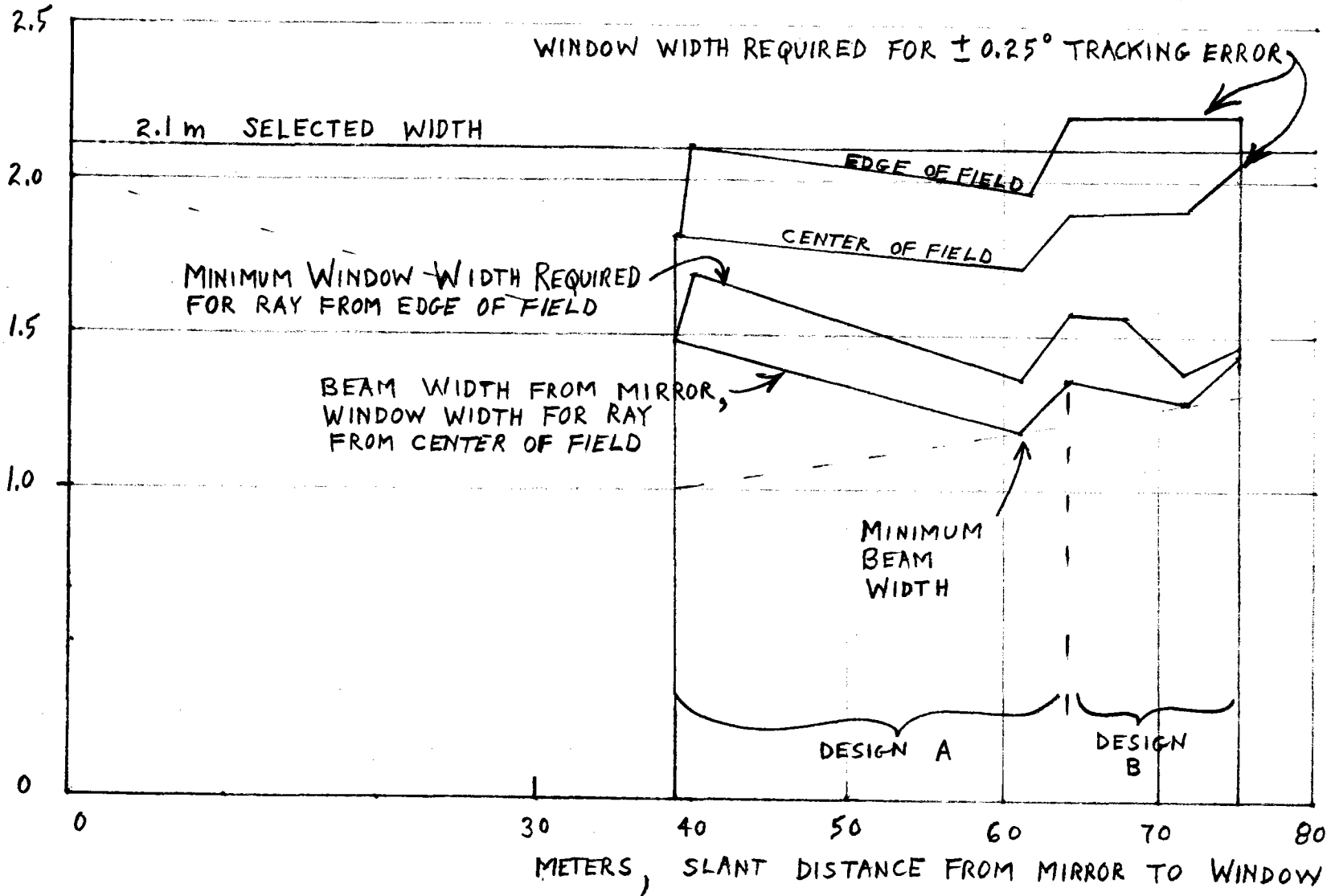
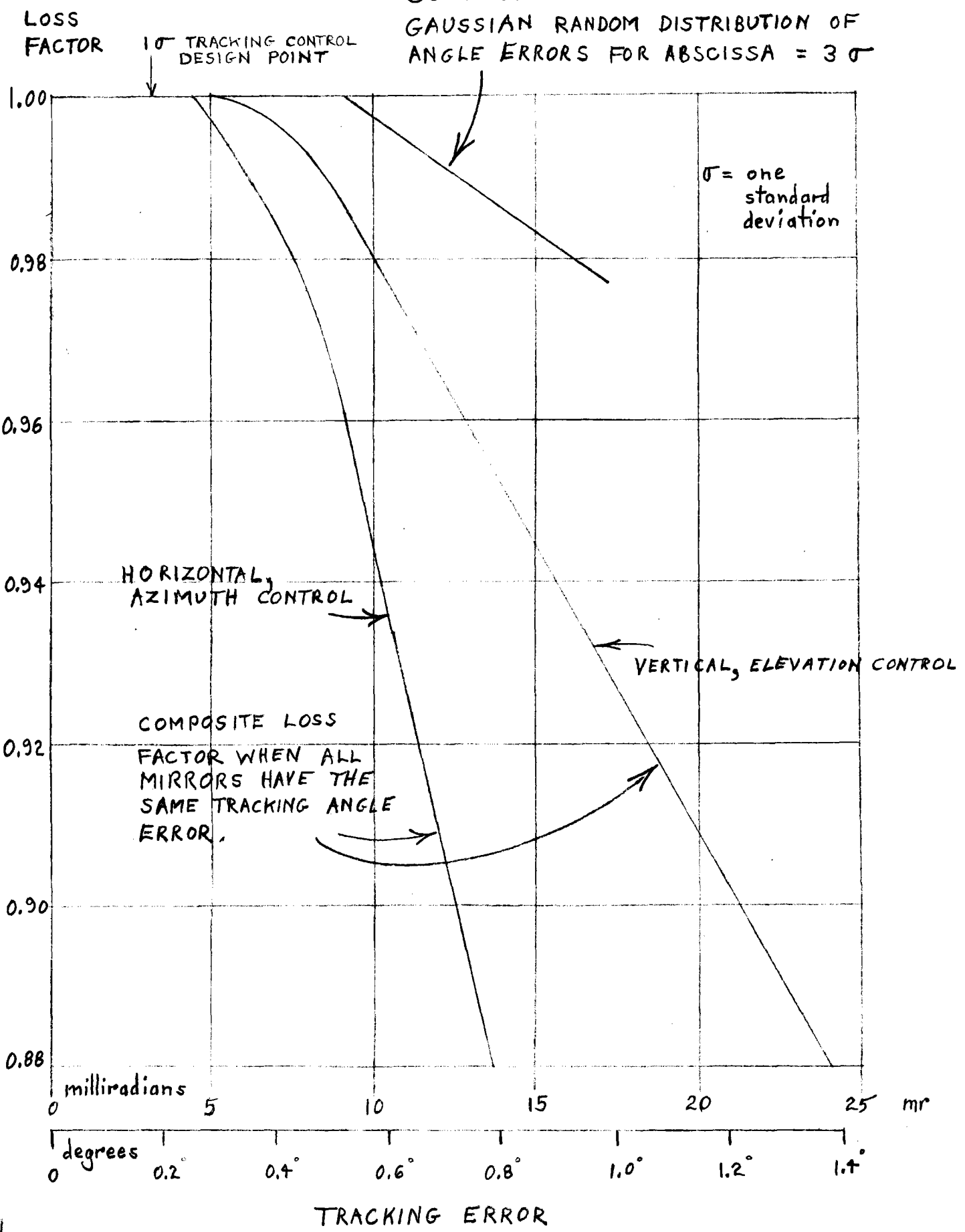
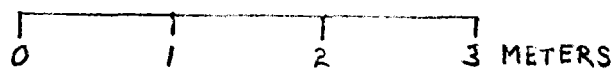
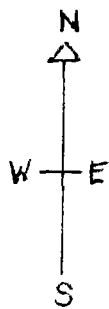
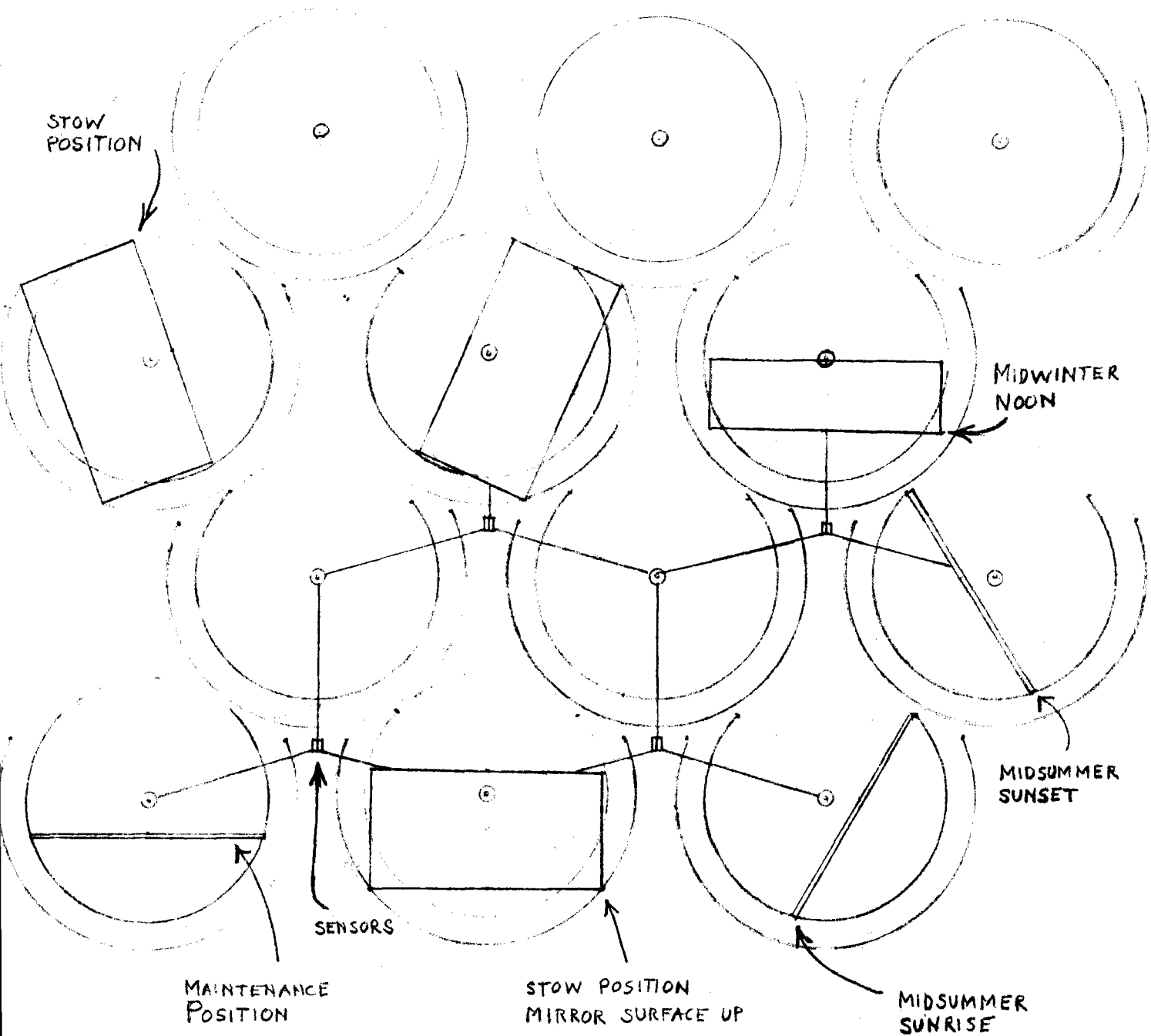


FIG. 10
O,J,M,S. 12 OCT. 75

COMPOSITE LOSS FACTOR FOR GAUSSIAN RANDOM DISTRIBUTION OF ANGLE ERRORS FOR ABSCISSA = 3σ





EXTREME RADII ROTATIONS
OF HELIOSTAT MIRRORS

FIG. 13
 MIDWINTER SUNRISE
 ELEVATION VIEW
 LOOKING SOUTHWEST
 8:30 a.m. Local Time
 31.8° N. Lat.

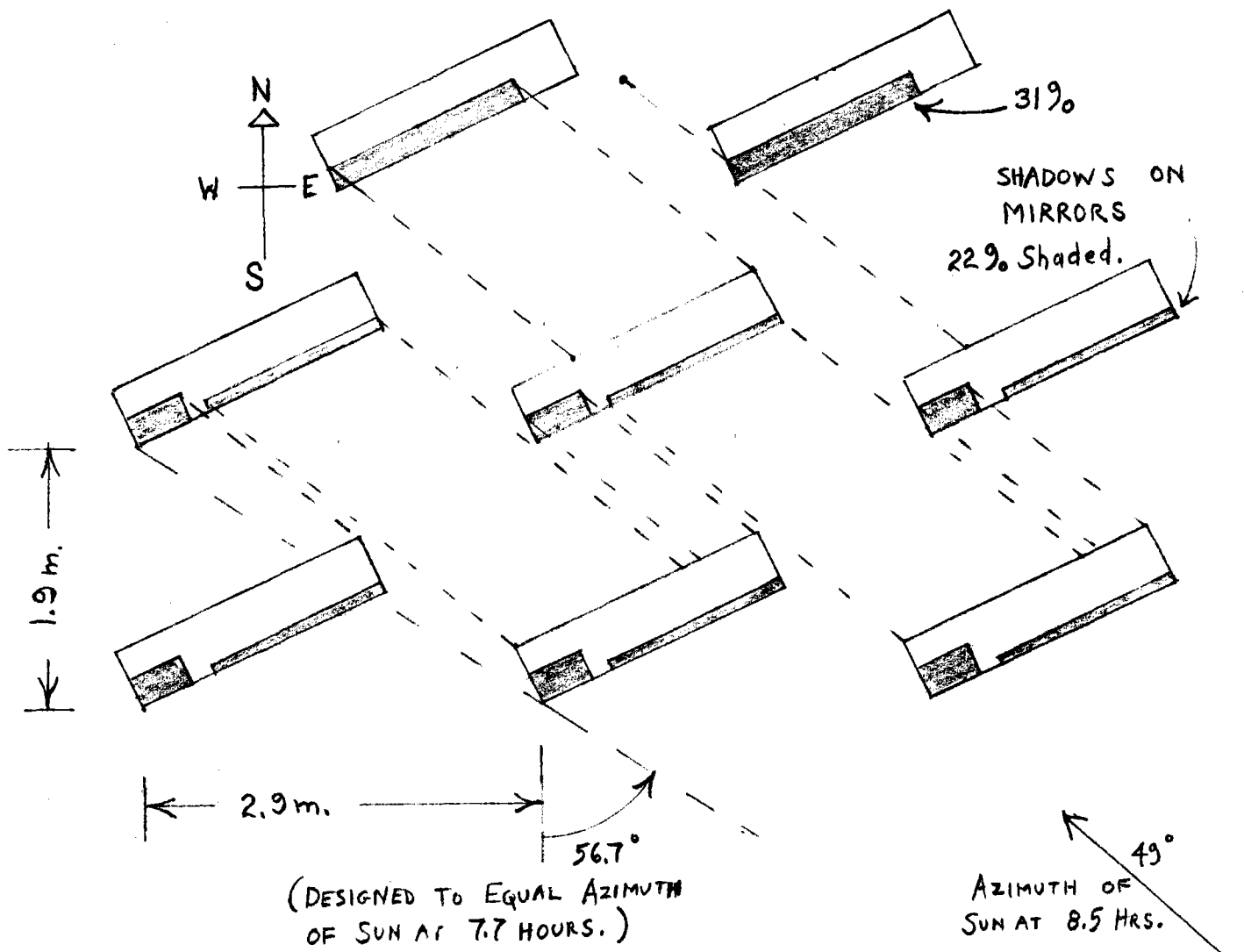
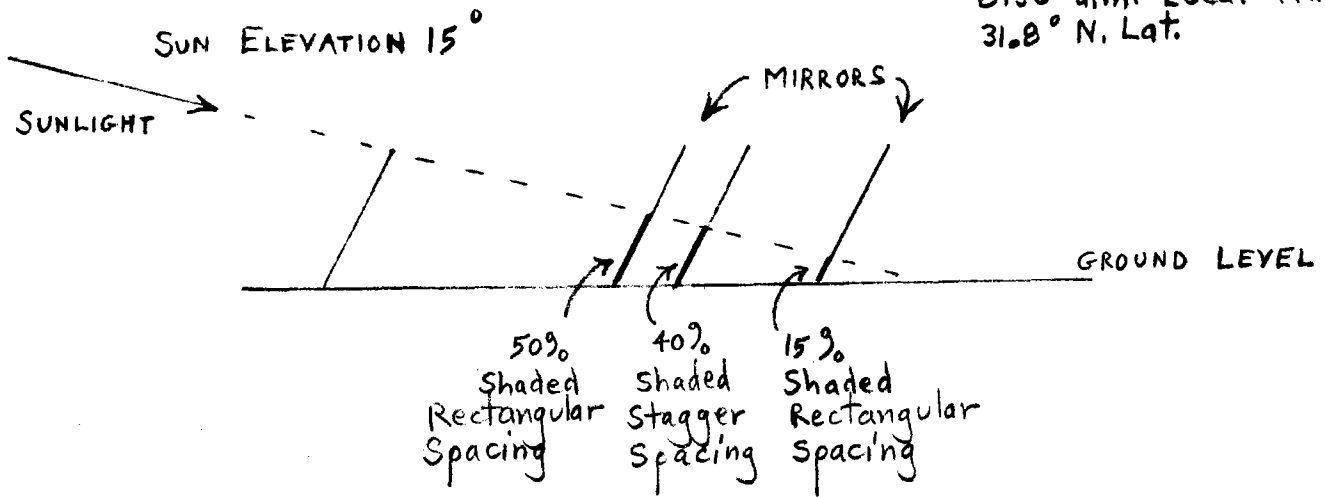


FIG. 14. PLAN VIEW OF MIRRORS MIDWINTER SUNRISE
 EL PASO, TEXAS 31.8° N. LAT. 8:30 a.m. Local Sun Time

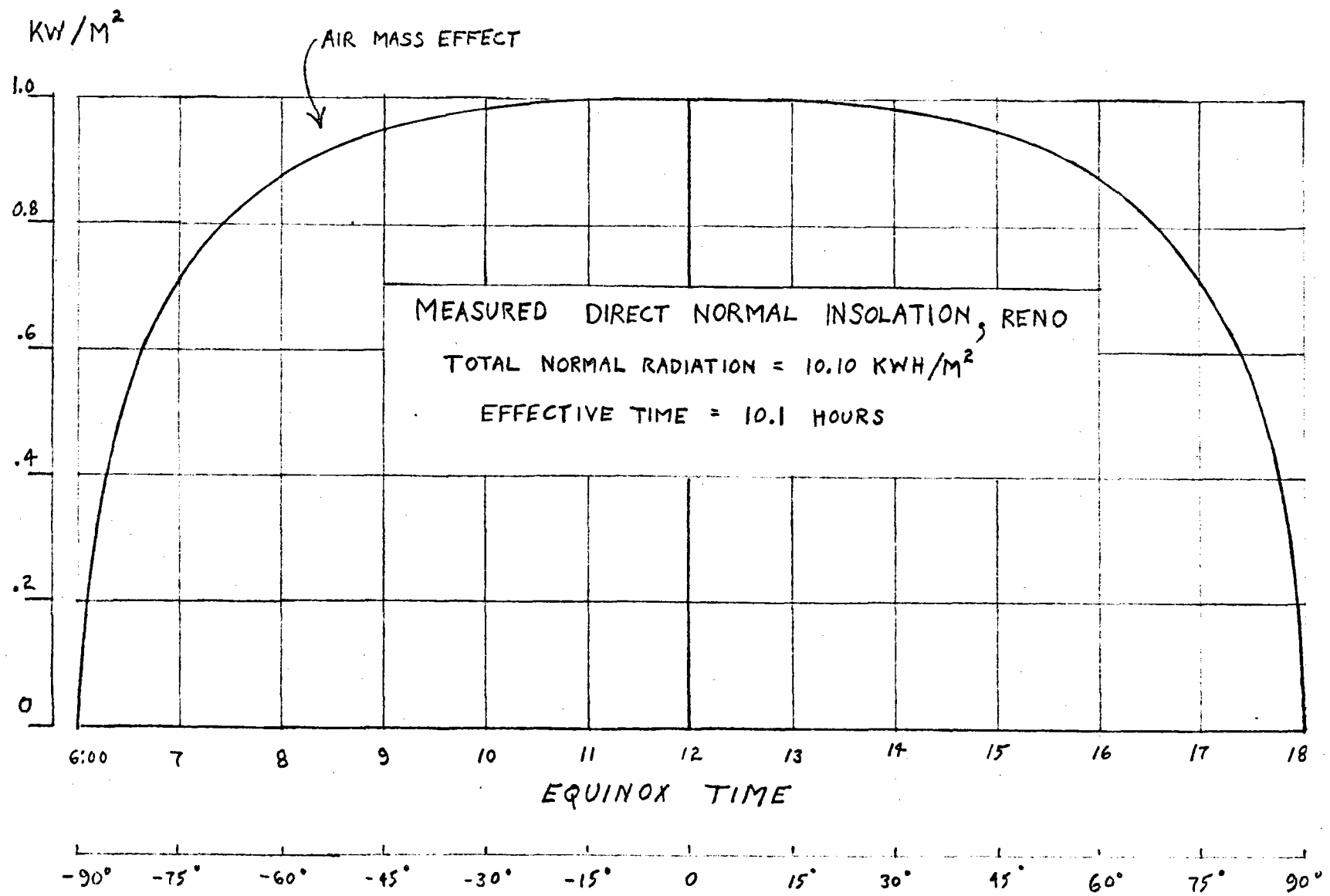
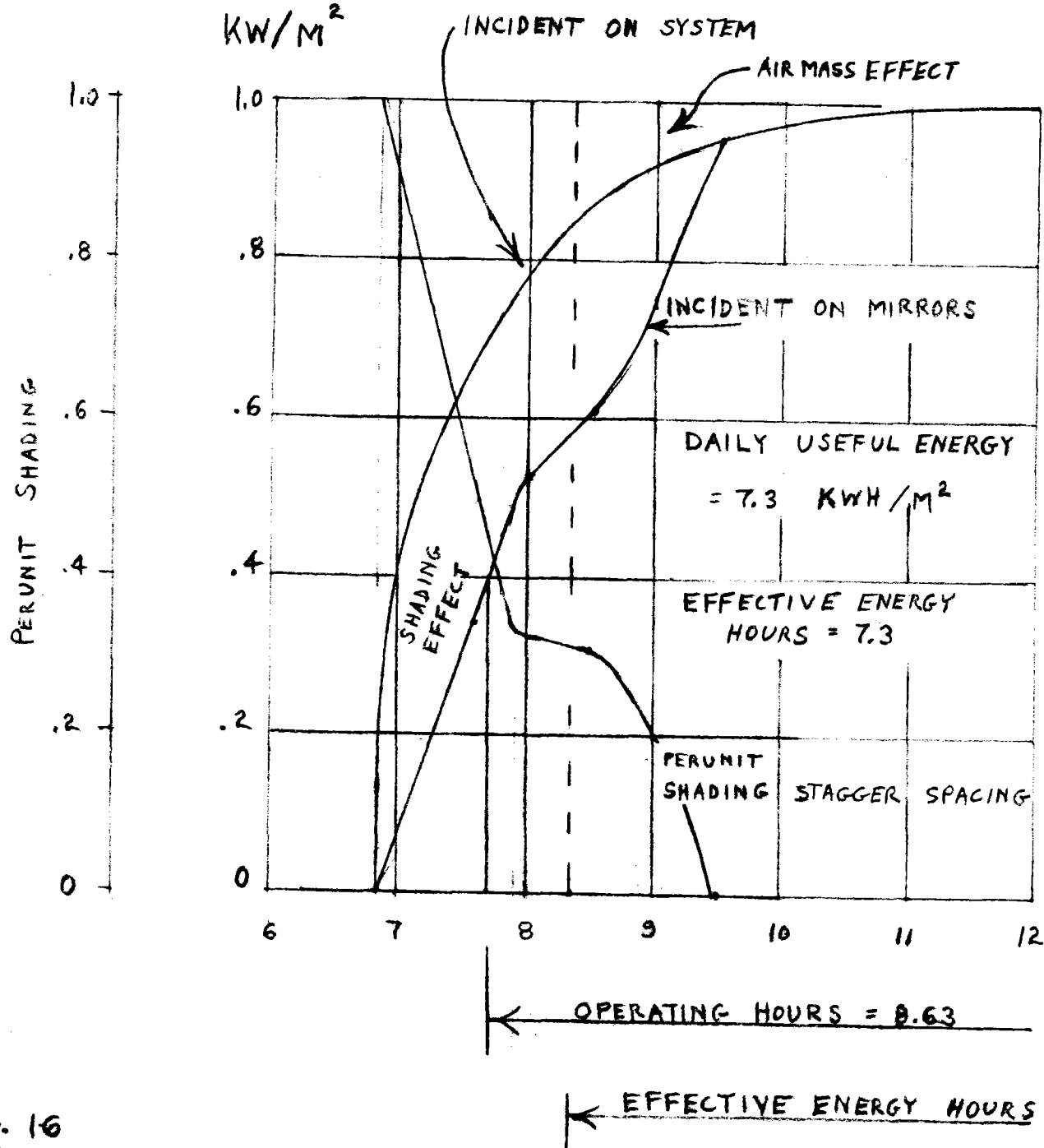


FIG. 15
O J M S 12 OCT. 75

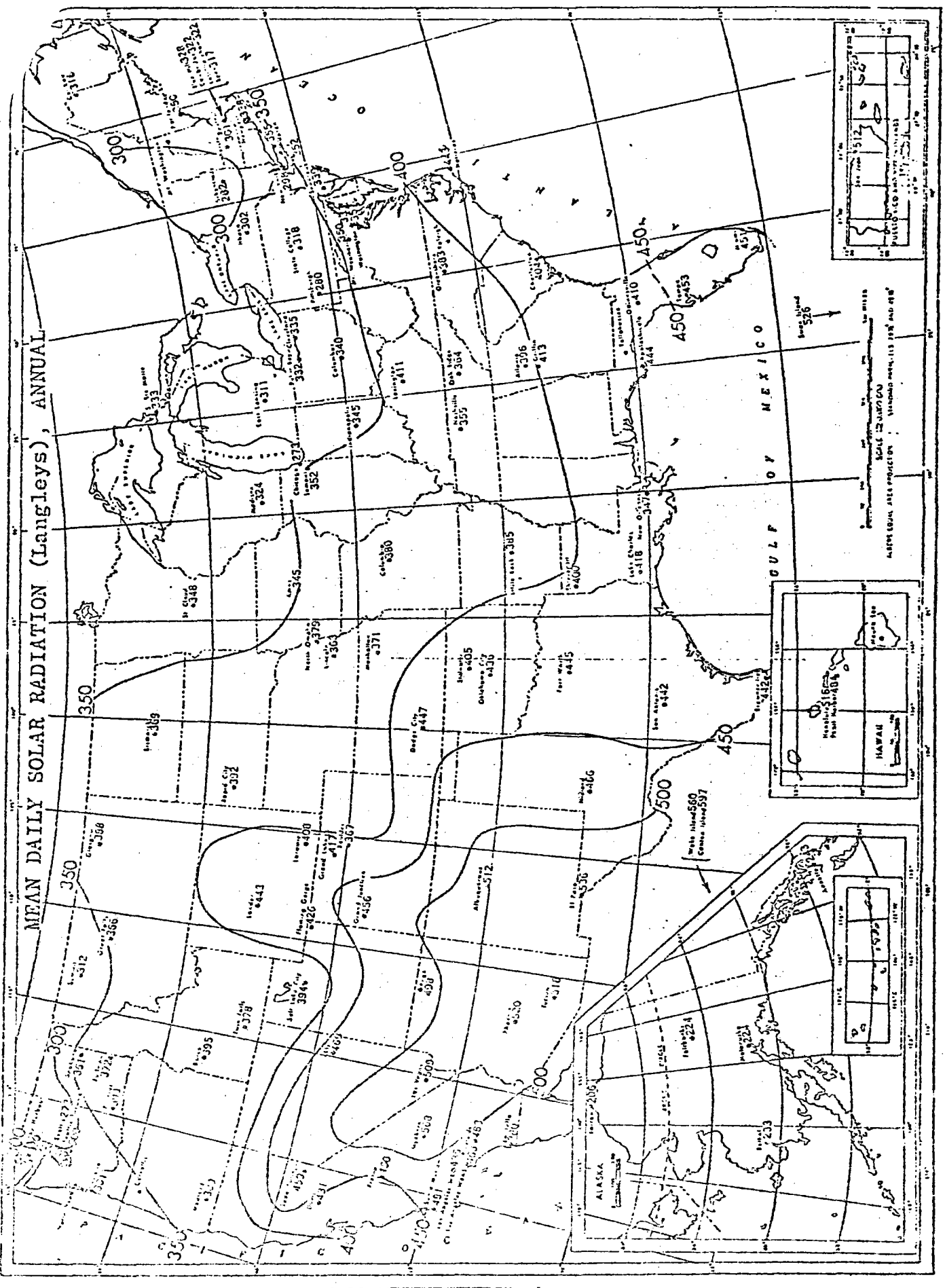


SHADING EFFECT
ON
DIRECT
NORMAL
INSOLATION

LOCAL SUN TIME
MIDWINTER
31.8° N. LATITUDE

FIG. 16
O.J.M.S. 12 OCT. 75

MEAN DAILY SOLAR RADIATION (Langley's), ANNUAL



SCALE IN LANGLEY'S
AN EQUAL AREA PROJECTION STANDARD MERIDIAN LONGITUDE 105° AND 95°

HAWAII
Peak 19,684'

1950

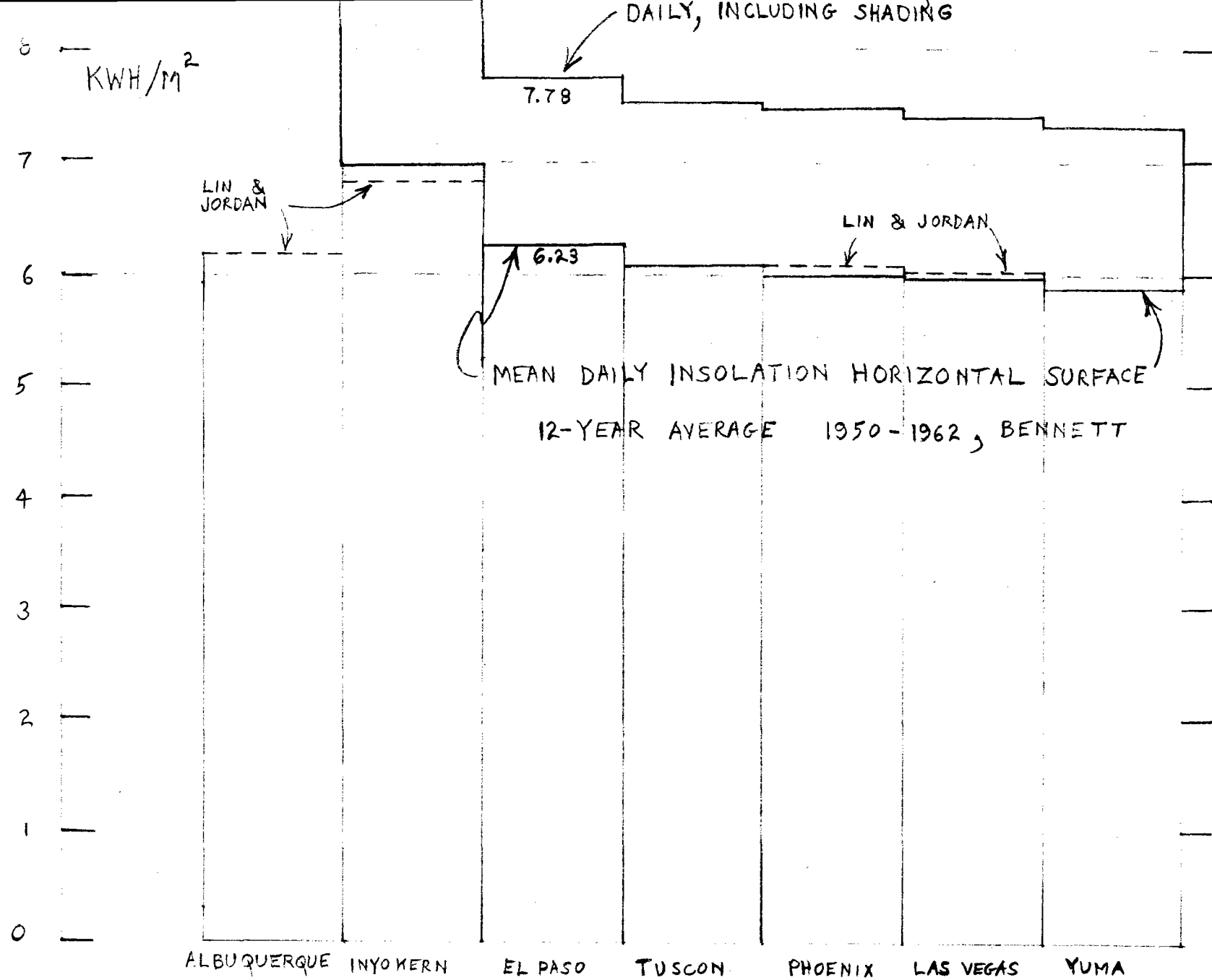


FIG. 18
O.J.M.S. 12 OCT. 75

KW/M²

DIRECT NORMAL MIDDAY INSOLATION

MONTHLY AVERAGES

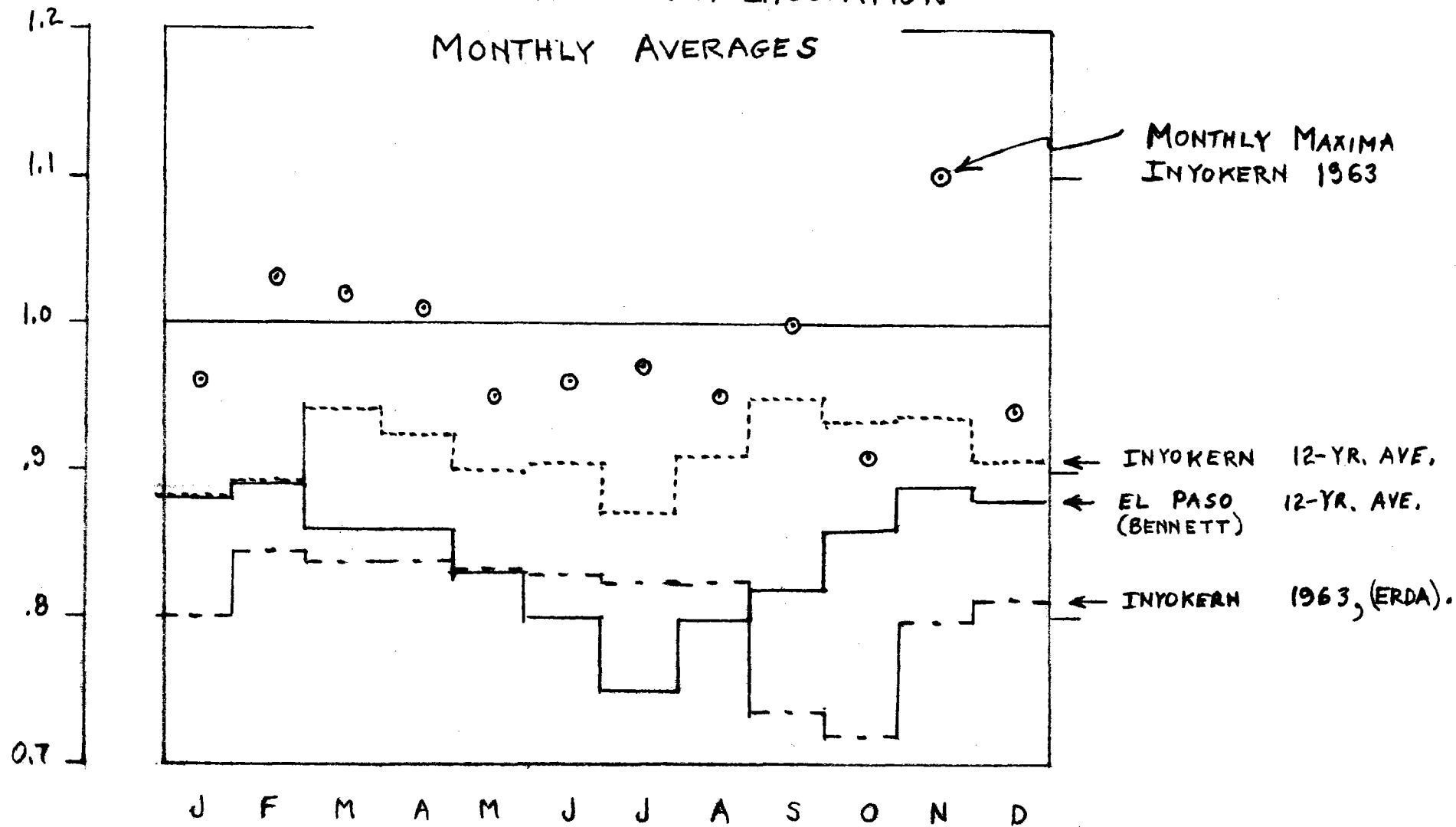


FIG. 19

O.N.M.S. 12 OCT. 75

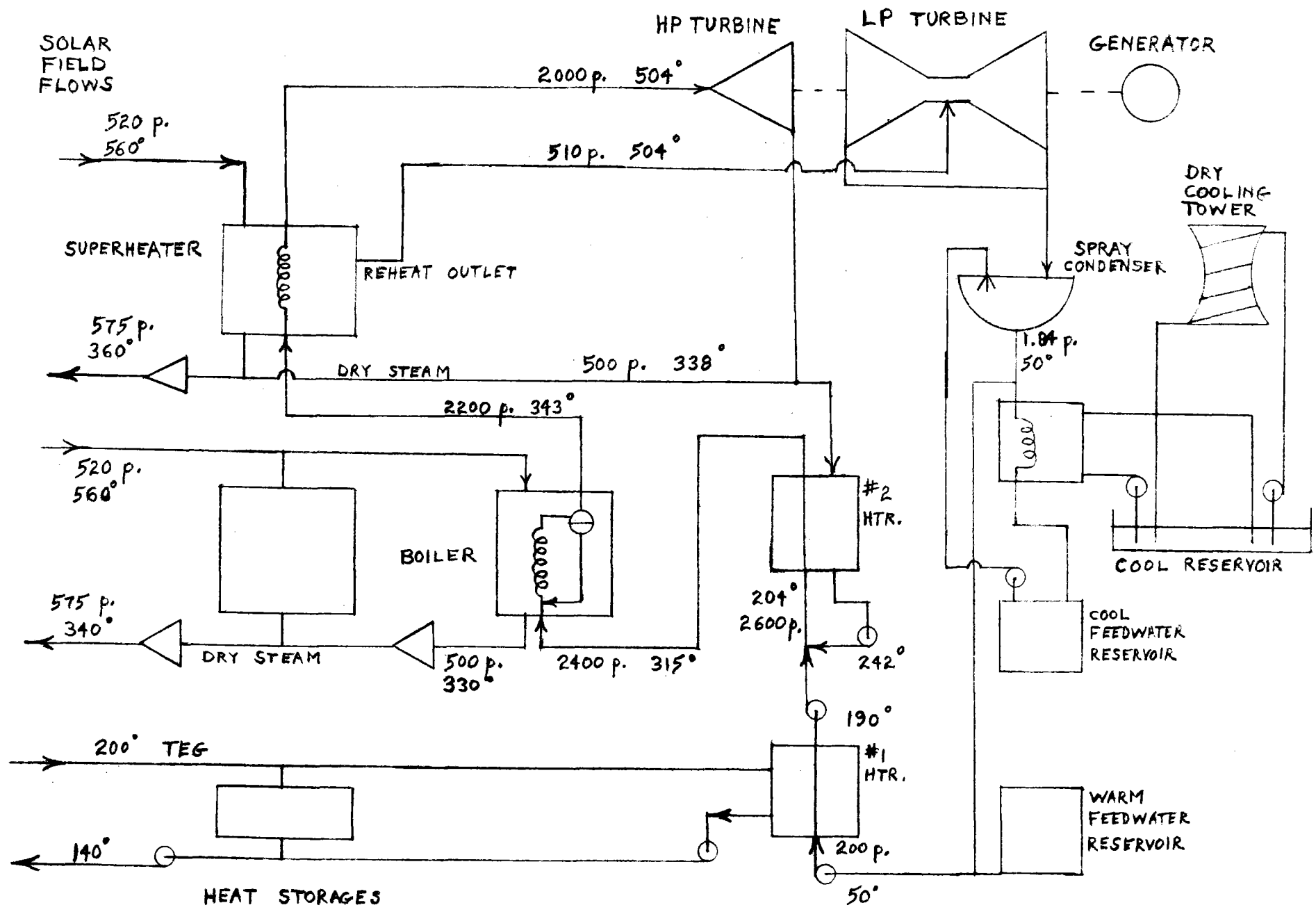
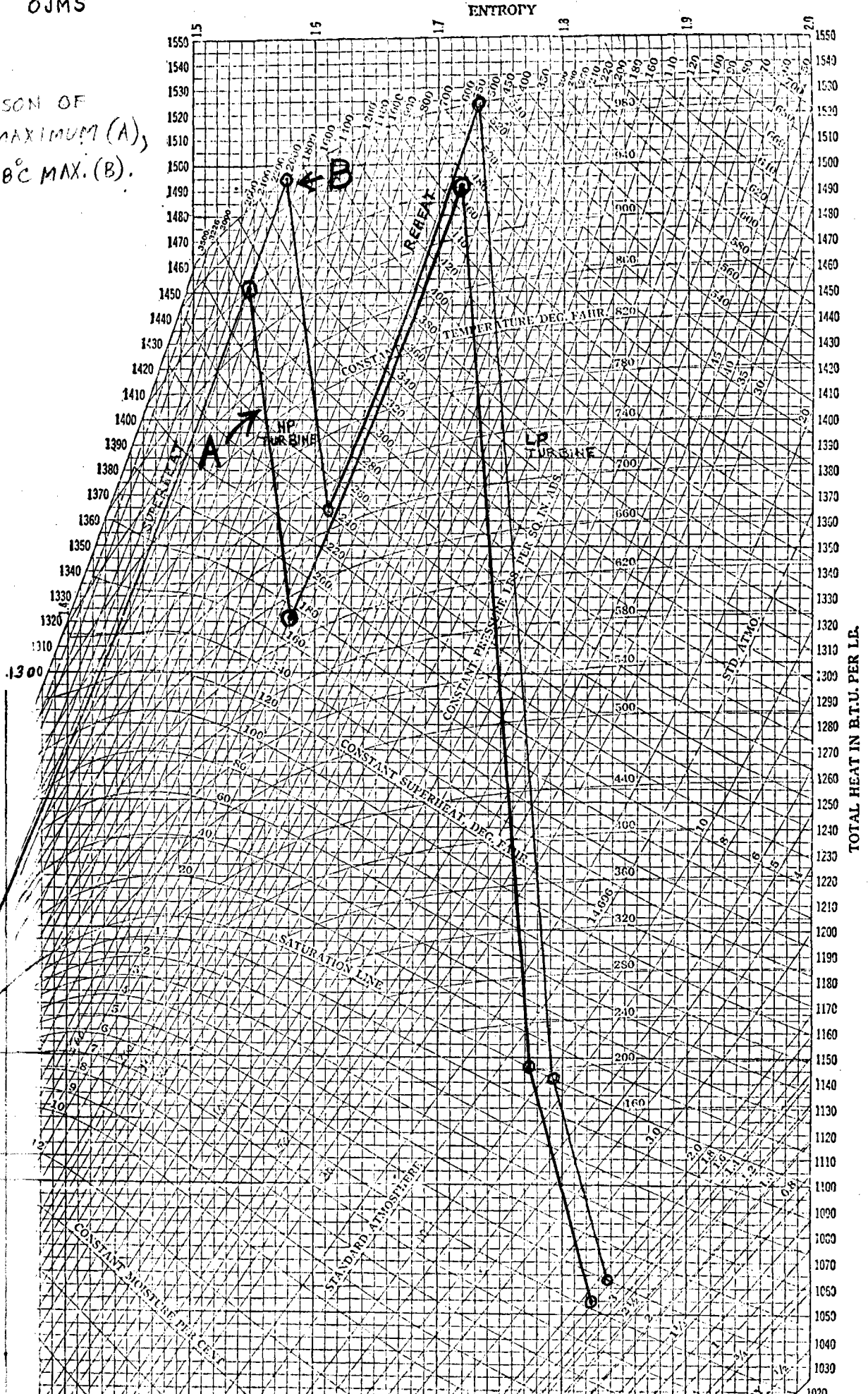


FIG. 20 SMITH SOLAR ELECTRIC PLANT; DAY STEAM CYCLE

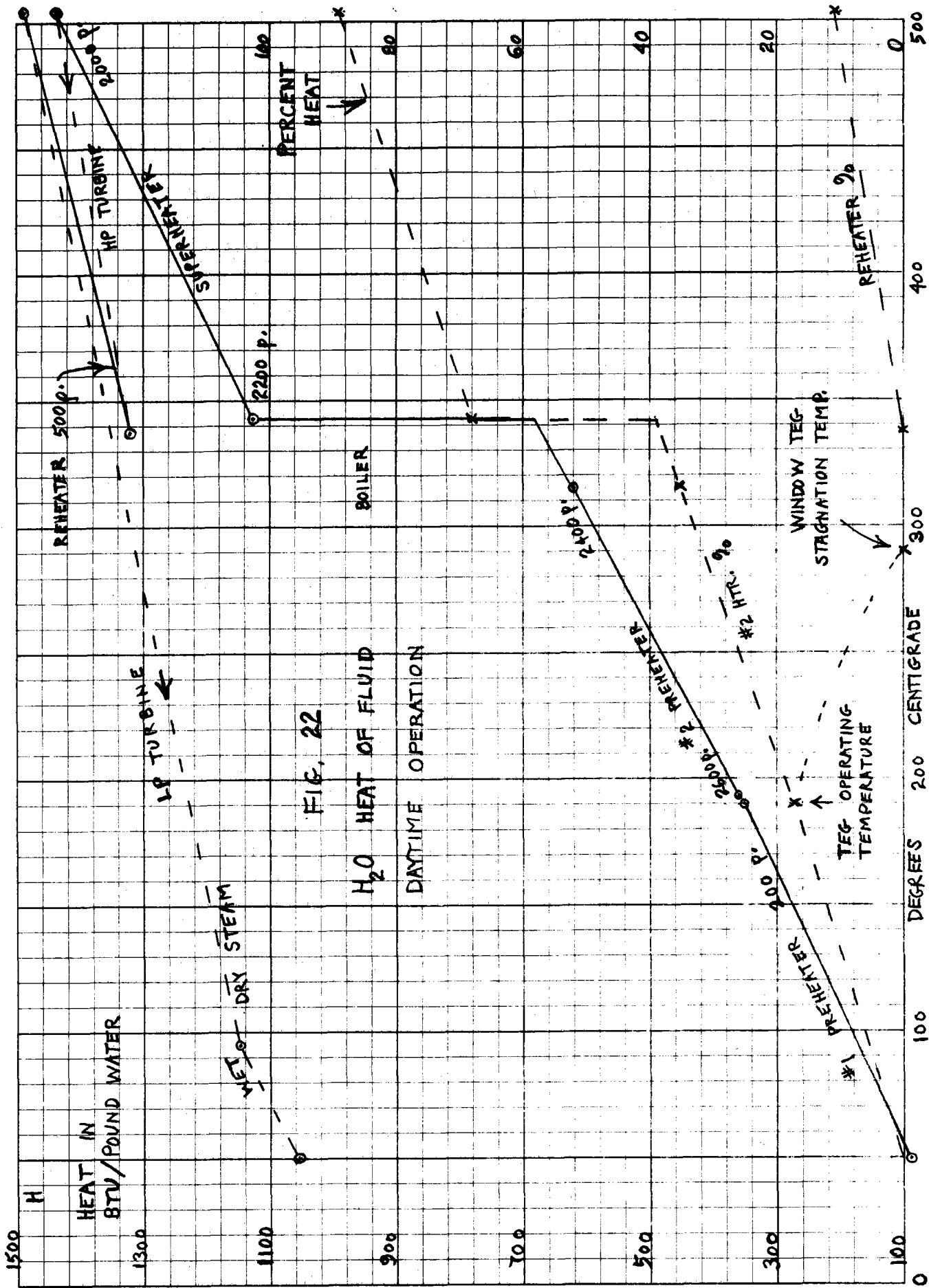
29 NOV. 75
OJMS

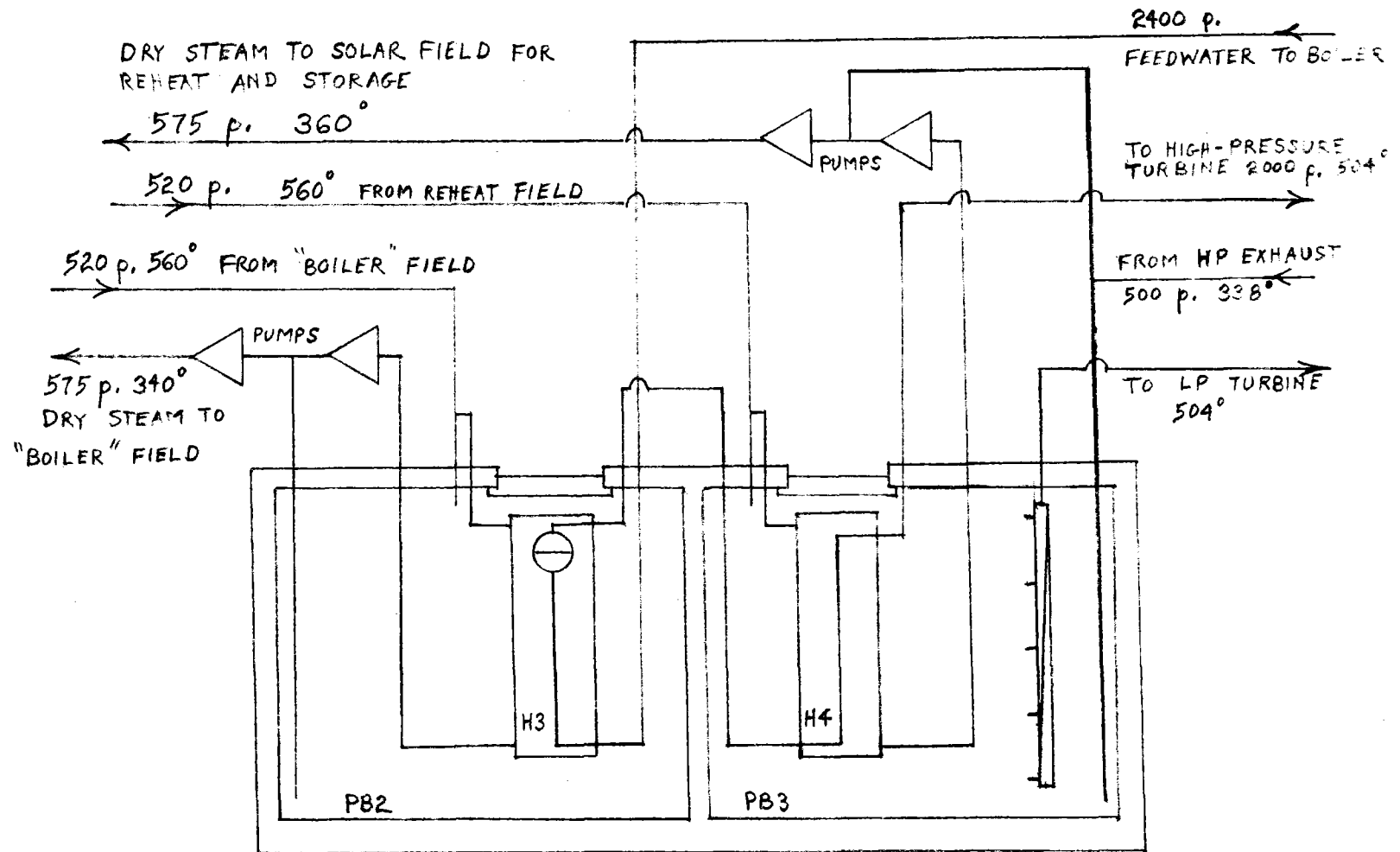
FIG. 21 MOLLIER DIAGRAM OF STEAM SYSTEM

COMPARISON OF
504°C MAXIMUM (A),
AND 538°C MAX. (B).



TOTAL HEAT IN B.T.U. PER LB.



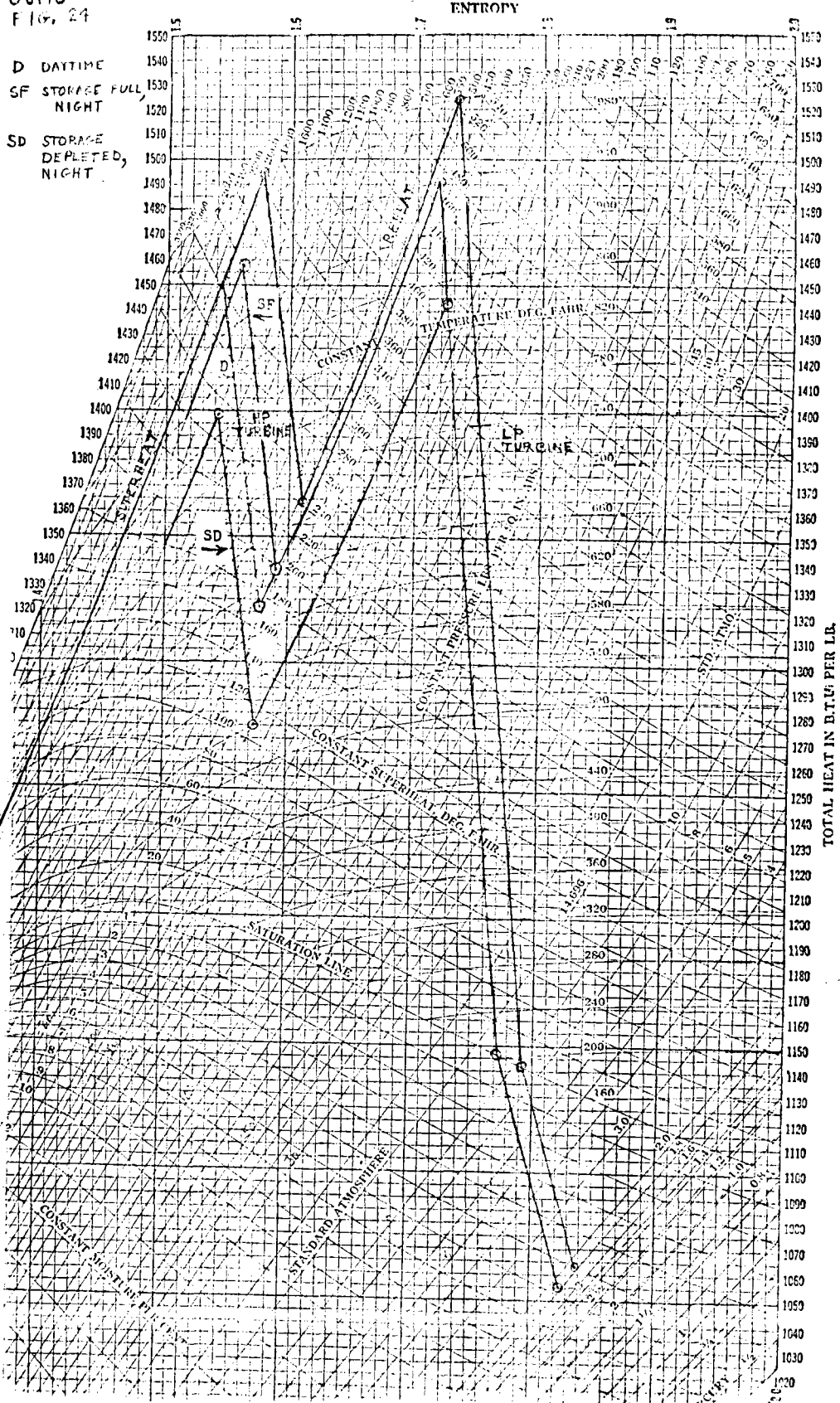


- H3 BOILER HEAT EXCHANGER
- H4 SUPERHEATER HEAT EXCHANGER
- PB2 BOILER HEAT STORAGE PEBBLE BED, 5600 TONS PER STORAGE HOUR
- PB3 SUPERHEATER HEAT STORAGE PEBBLE BED, 4950 TONS PER STORAGE HOUR FOR 450 MWH STORAGE, 40 m. DIAMETER BY 25 m. HIGH.

FIG. 23 PRESSURIZED HEAT STORAGE RESERVOIR

29 NOV. 75
OJMS
FIG. 24

MOLLIER DIAGRAM OF STEAM SYSTEM



D DAYTIME
SF STORAGE FULL
NIGHT
SD STORAGE
DEPLETED,
NIGHT

FIG. 25

SENSIBLE HEAT STORAGE REQUIREMENTS

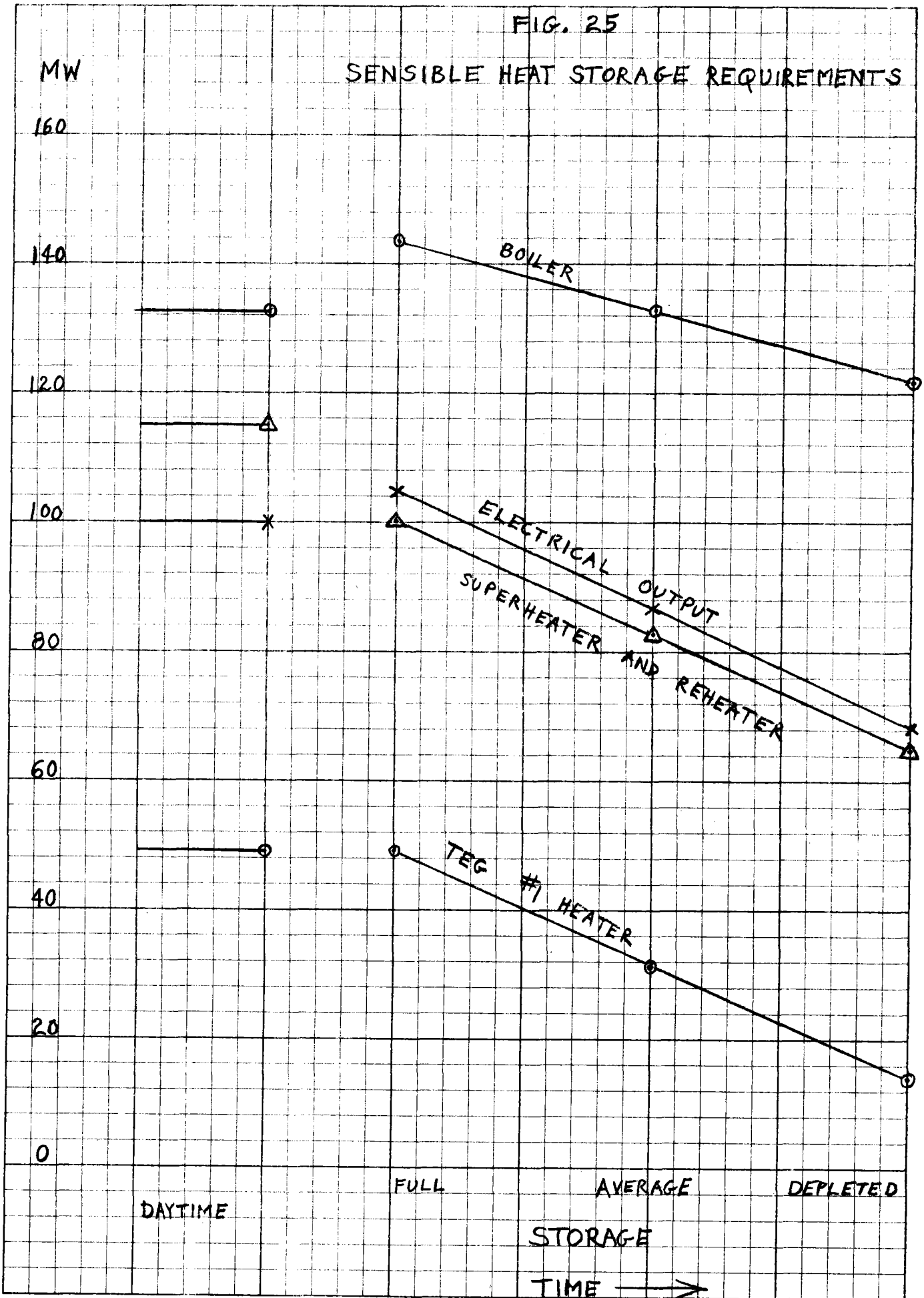


FIG. 26

FUSION STORAGE CHARACTERISTICS

MW_e

HEAT AVAILABLE FROM SOLAR FIELD FLUID

300

FUSION HEAT STORAGE CHARACTERISTIC

TURBINE STEAM REQUIREMENTS AT 100 MW_e FROM FUSION STORAGE

250

200

150

100

50

0

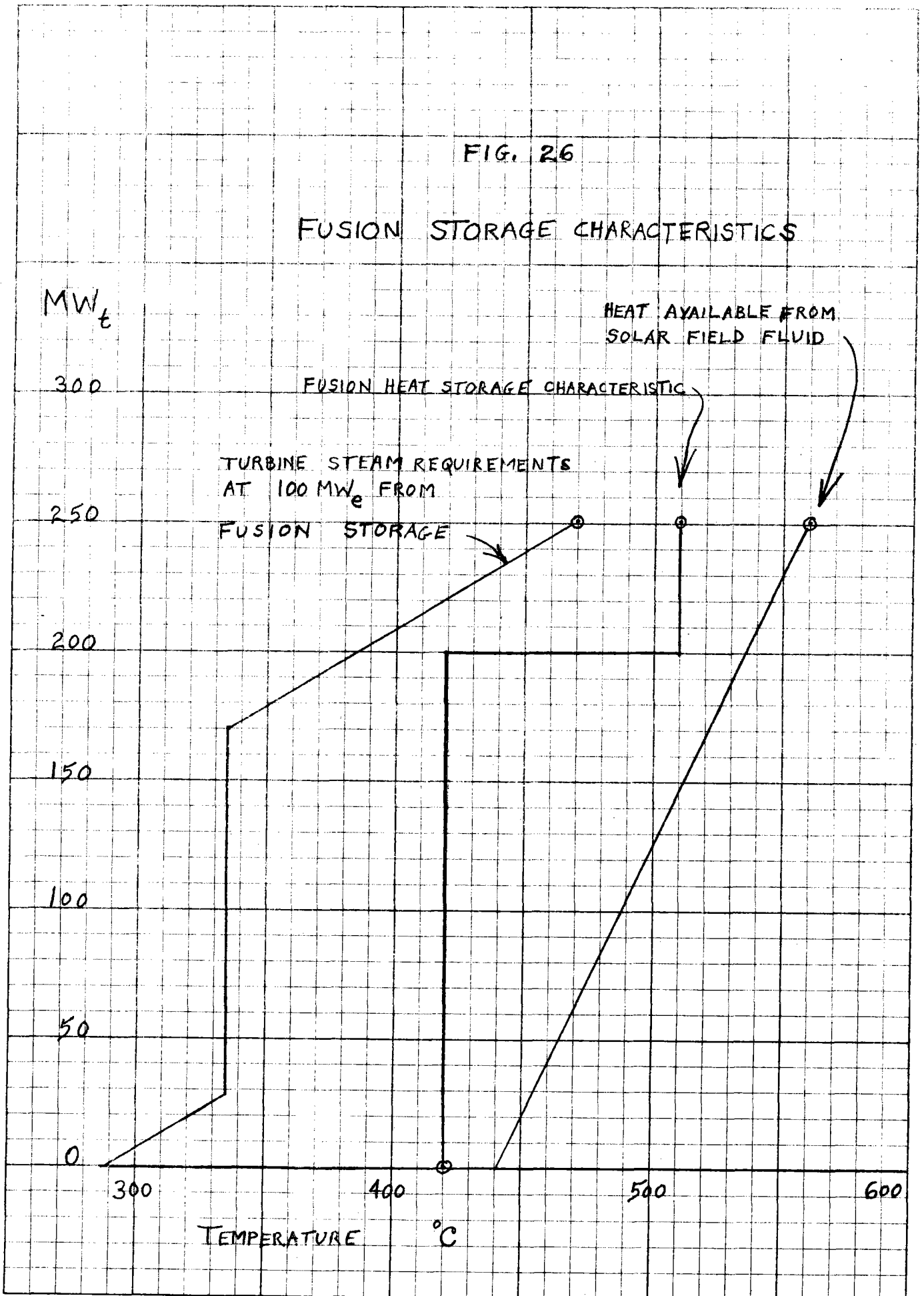
300

400

500

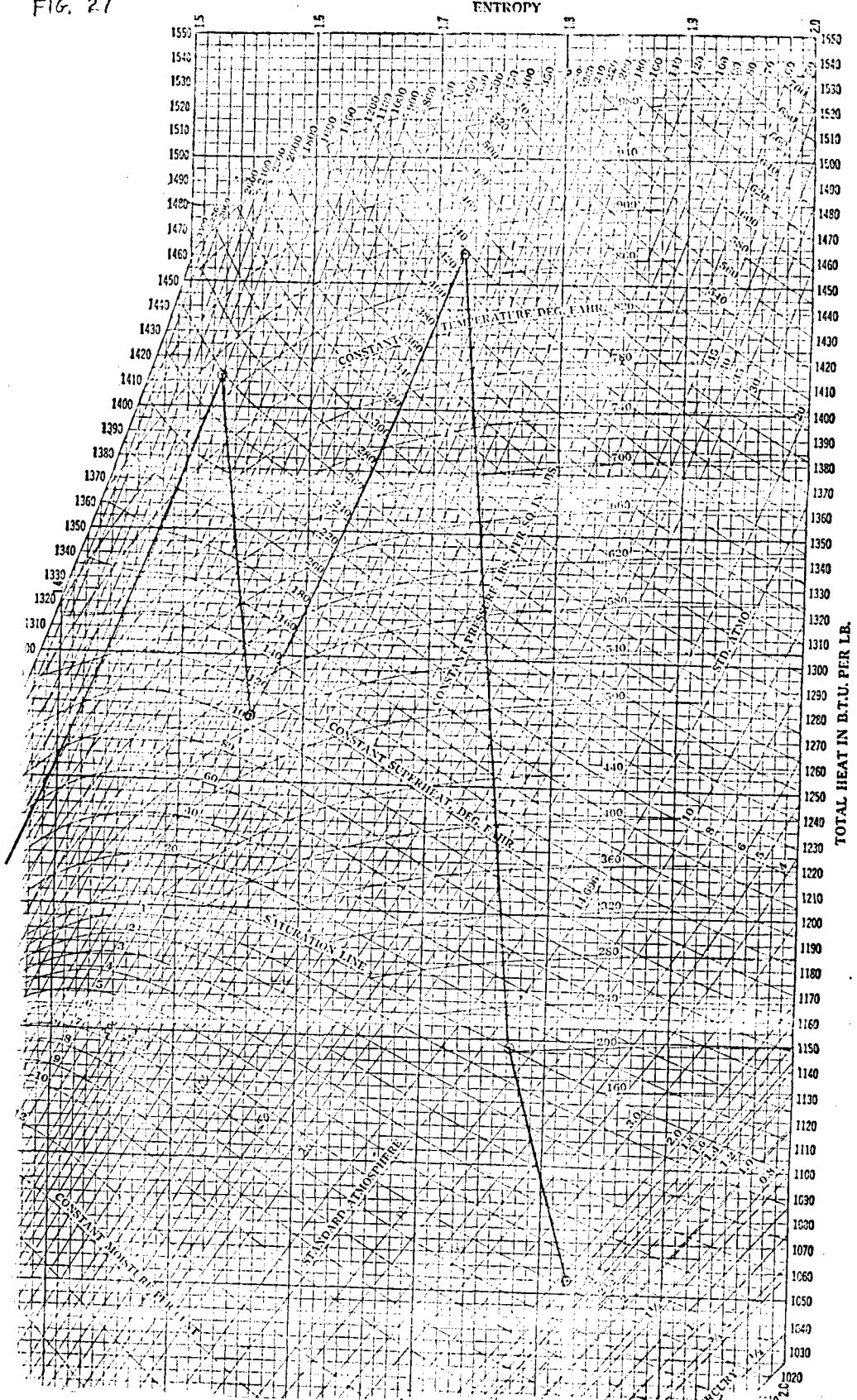
600

TEMPERATURE °C



OJMS.
13 DEC. 75
FIG. 27

STEAM CYCLE FOR OPERATION FROM FUSION STORAGE



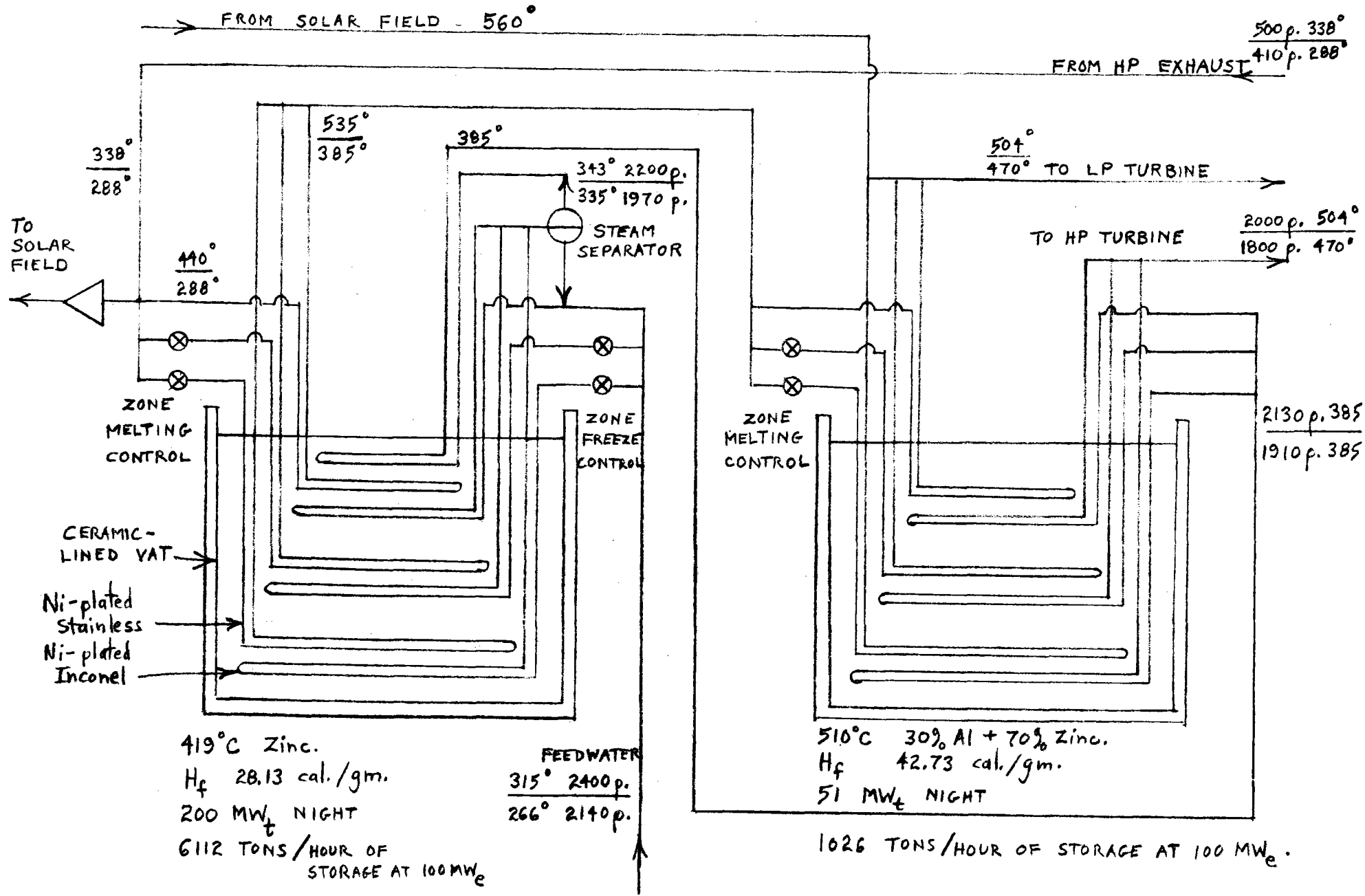


FIG. 28 FUSION STORAGE SYSTEM

OJMS, 13 DEC. 75

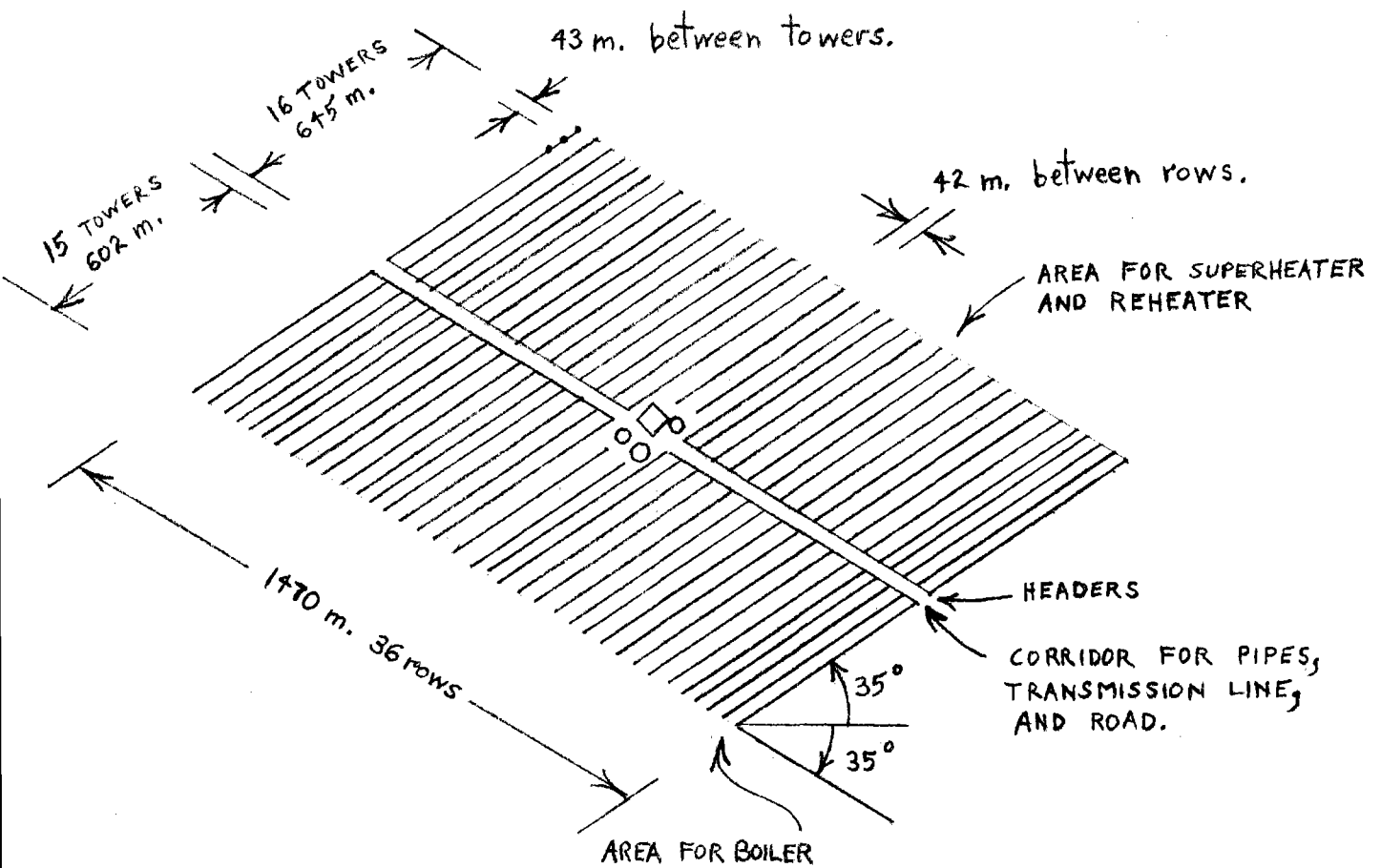
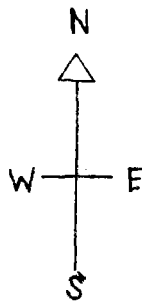


FIG. 29

PIPING TREE

1100 TOWERS

1.9 KM² OF ACTIVE HEXAGON AREA

47.8 KM TREE "LENGTH"

MONASH UNIVERSITY, MELBOURNE, AUSTRALIA (1966 to 1967)

Senior Research Fellow in Economics and Engineering. Fast Load Flows and Input-Output Models.

TECHNISCHE HOCHSCHULE DARMSTADT, WEST GERMANY (1960)

Guggenheim Fellow, Non-linear Control System, Two-Field Synchronous Generators.

INSTITUTO TECNOLOGICO DE AERONAUTICA, SAO JOSE DOS CAMPOS,
SAO PAULO, BRASIL (1954 to 1956)

Professor of Electronics, Automatic Control, and Statistical Synthesis.

SUMMIT CORPORATION, SCRANTON, PENNSYLVANIA (1945 to 1947)

Phonograph Records.

WESTINGHOUSE RESEARCH LABORATORIES, FOREST HILLS,
PENNSYLVANIA (1944 to 1945)

X-ray and microwave measurements, magnetrons, radiation detectors.

DENVER UNIVERSITY, DENVER, COLORADO (1943 to 1944)

Assistant Professor, automatic control, microwaves.

TUFTS COLLEGE, MEDFORD MASSACHUSETTS (1941 to 1943)

Instructor, power and high voltage.

H. J. RYAN HIGH VOLTAGE LABORATORY, STANFORD UNIV. (1938 to 1941)

Research Assistant.

Consultant at various times for:

Hewlett Packard Company

Sacramento Municipal Utility District

Shell Development Company

International Business Machines Research Laboratory

Industrial Nucleonics

Hamilton Standard Division of United Aircraft

ElectroScientific Instruments

Lear-Siegler

Teknekron, Inc.

Consolidated Systems Corporation

Donner Scientific Company

Lockheed Aircraft, Inc.

Doble Engineering Company

RISCO Company

AFFILIATIONS:

Fellow, IEEE and AAAS.

Member, ASEE, SSRS, ISA, Sigma Xi, Phi Kappa Phi, Tau Beta Pi, Eta Kappa Nu, Phi Lambda Upsilon, and Phi Eta Sigma.

PATENTS:

13 Patents issued to Otto J. M. Smith on power system control, measuring apparatus, and generators.

PUBLICATIONS:

Over 130 publications in reviewed journals, on measurement, control, stability, power systems, optimization, economics, computer programming, and industrial electronics.

SELECTED REFERENCES:

Power System with Transient Control and Method, U.S. Patent 3,529,174, Sept. 15, 1970.

System, Apparatus and Method for Improving Stability of Synchronous Machines, U.S. Patent 3,388,305, June 11, 1968.

System and Method for Alternating Current Machines and Apparatus Therefore, U.S. Patent 3,483,463, December 9, 1969.

Sine Wave Generator, U.S. Patent 2,148,278, May 29, 1956.

Characterization of Equilibrium and Stability in Power Systems, Equilibrium Analysis of Power Systems, and Stability Analysis of Power Systems, all coauthored with Carlos Tavora, IEEE Trans. PAS, Vol. PAS-91, No. 3, pp. 1127-1144, May/June, 1972.

Series Capacitor Switching to Quench Electromechanical Transients in Power Systems, and Rotor Velocity Measurement from Power Balance Analog, both coauthored with Ajit Mane and Richard Webster, IEEE Trans. PAS, Vol. PAS-90, No. 2, pp. 427-440, March/April 1971.

Solar Power Plant Based On Rankine Cycle. coauthored with Calin Mihaileanu and Mihai G. M. Pop. Energetica. Bucuresti, Romania, Volumul XXIII, No. 1, Ianuarie, 1975, pp. 1 - 10.

MIRROR SURFACE

SHELD AHL G - 400300

2 MIL POLYESTER BASE (MYLAR OR MELANEX)

FIRST SURFACE SILVERED 700 ANGSTROMS SILVER WITH

MONOLAMIC 822 (ACRYLIC BASE) COVERING

TAUT MEMBRANE: 0.95 REFLECTANCE SPECULAR

(60% WITHIN 5 MILLIRADIANS)

GERALD P. MASS, MARKETING MANAGER

DR. DON ANDERSON,

MR. RON NICCUM

SHELD AHL INC.

P. O. BOX 170

NORTHFIELD, MINNESOTA, 55057

507-645-5631

CHART 6

PERTINENT PHYSICAL PROPERTIES OF TRANSPARENT GLAZING MEDIA				
GLAZING MEDIA	REFRACTIVE INDEX	**SOLAR ENERGY TRANSMISSION (PER SHEET)	**SOLAR ENERGY LOSSES PER SHEET (2 SURFACE REFLECTION PLUS ABSORPTION)	***MAXIMUM OPERATING TEMP.
SHEET LIME GLASS (LOW IRON OXIDE CONTENT 0.05% TO 0.06%)	1.51	DS (3.2 mm) - 87% 3/16" (4.8 mm) - 85%	13% (8.1%R + 4.9%A) 15% (8.0%R + 7.0%A)	400° F (204°C)
WATER-WHITE CRYSTAL GLASS #76 (0.01% IRON OXIDE)	1.50	5/32" (4.0 mm) - 91% 3/16" (4.7 mm) - 90.5% 7/32" (5.5 mm) - 90%	9% (8.0%R + 1.0%A) 9.5% (8.0%R + 1.5%A) 10% (8.0%R + 2.0%A)	400° F (204°C)

PERTINENT PHYSICAL PROPERTIES OF TRANSPARENT GLAZING MEDIA

GLAZING MEDIA	NOMINAL THICKNESS	NOMINAL MAXIMUM SIZES RECOMMENDED	WEIGHT (LBS./SQ.FT.)	EXPANSION COEFFICIENT
SHEET LIME GLASS (LOW IRON OXIDE CONTENT 0.05% TO 0.06%)	DS (1/8")	34" x 76"	1.63	50 x 10 ⁻⁷ PER ° F
	3/16"	36" x 96"	2.51	
WATER-WHITE CRYSTAL GLASS #76 (0.01% IRON OXIDE)	5/32"	34" x 76"	2.03	47 x 10 ⁻⁷ PER ° F
	3/16"	36" x 96"	2.41	
	7/32"	48" x 96"	2.80	

CHART 7A

PERTINENT PHYSICAL PROPERTIES OF TRANSPARENT GLAZING MEDIA

GLAZING MEDIA	NOMINAL THICKNESS	NOMINAL MAXIMUM SIZES RECOMMENDED	WEIGHT (KGS/SQ.METER)	EXPANSION COEFFICIENT
SHEET LIME GLASS (LOW IRON OXIDE CONTENT 0.05% TO 0.06%)	3.2 mm	86.4 cm x 193 cm	7.96	90 x 10 ⁻⁷ PER ° C
	4.8 mm	91.4 cm x 244 cm	12.25	
WATER-WHITE CRYSTAL GLASS #76 (0.01% IRON OXIDE)	4.0 mm	86.4 cm x 193 cm	9.91	85 x 10 ⁻⁷ PER ° C
	4.7 mm	91.4 cm x 244 cm	11.77	
	5.5 mm	122 cm x 244 cm	13.67	

PERTINENT PHYSICAL PROPERTIES OF TRANSPARENT GLAZING MEDIA

GLAZING MEDIA	ELASTIC MODULUS	DESIGN TENSILE STRENGTH	HEAT DEFLECTION TEMPERATURE	
SHEET LIME GLASS (LOW IRON OXIDE CONTENT 0.05% TO 0.06%)	10.5×10^6 psi	**Annealed: 1600 psi **Tempered: 6400 psi	In Excess of 1100° F.	Steel ball impact per ANSI Z26.1-1966 requires testing 12" x 12" samples. Fully Tempered glass must withstand 10' drop of 1/2 lb. steel ball (5 ft.lbs. impact). Also, it must withstand soft body impact of 11 lb. shot bag dropped 8'. (88 ft.lbs. impact). 1/8" Fully Tempered glass and thicker will withstand these tests, temperature level having little effect on this performance.
WATER-WHITE CRYSTAL GLASS #76 (0.01% IRON OXIDE)	10.5×10^6 psi	**Annealed: 1600 psi **Tempered: 6400 psi	In Excess of 1100° F.	
SHEET LIME GLASS (LOW IRON OXIDE CONTENT 0.05% TO 0.06%)	0.738×10^6 kgs/sq. cm.	**Annealed: 112.5 kgs/sq.cm. **Tempered: 450 kgs/sq.cm.	In Excess of 600° C	Steel ball impact per ANSI Z26.1-1966 requires testing 30.5cm x30.5cm samples. Fully Tempered glass must withstand 3.05 m drop of 0.227 kg steel ball (0.69 kg-m impact). Also it must withstand soft body impact of 4.99 kg shot bag dropped 2.44m (12.2 kg-m impact). 3.2 mm Fully Tempered glass and thicker will withstand these tests, temperature level having little effect on this performance.
WATER-WHITE CRYSTAL GLASS #76 (0.01% IRON OXIDE)	0.738×10^6 kgs/sq. cm.	**Annealed: 112.5 kgs/sq.cm. **Tempered: 450 kgs/sq.cm.	In Excess of 600° C	

Low Reflection Coatings

General Information

Reduce reflections on instrument dial covers and lenses.

Increase net transmission through one or a series of optical elements.

Glass has a reflectance of approximately 4% for each surface in the visible spectrum. Three types of low reflection coatings can be applied to plate glass ($N = 1.52$), optical glass, or IR window materials to achieve varying degrees of low reflection efficiency.

Regular Low Reflection Coating No. 525

Magnesium fluoride applied to reduce reflectance to less than 2% per surface in the range of greatest sensitivity as seen by the human eye fulfills the spectral and environmental requirements of MIL-C-675A. See Specification 1079, Coating No. 525.

HLR - Special Low Reflection Coating No. 526

is a multi-layer coating to reduce reflectance to less than .5% average from 450 to 625 millimicrons per surface.

Adherence

No visible part of the coating shall be removed by the cellulose tape test described here:

Test: The tacky surface of cellulose tape shall be carefully placed in contact with a portion of the coated surface and firmly rubbed against that surface. It shall then be quickly removed with a snap action that exerts the greatest possible stripping action on the coating.

Durability

No evidence of film removal or film abrasion shall result from one or both of the following tests:

- (a) The coated element shall be placed in a thermostatically controlled cabinet with a salt atmosphere at a temperature of 95°F. plus or minus 4°F. for 48 hours. The salt atmosphere shall be obtained by allowing a stream of air to bubble through a salt solution containing about 1½ pounds of sodium chloride per cubic foot of water.
- (b) The coated element shall be placed in a thermostatically controlled humidity cabinet with an atmosphere of at least 95% relative humidity and at a temperature of 120°F. plus or minus 4°F. for a continuous period of 24 hours.

Effect of Temperature

The coating shall function satisfactorily and shall not be damaged by exposure to an ambient temperature of minus 60°F and plus 500°F.

HEL R - Hi-Efficiency Low Reflection Coating No. 527

is a multi-layer coating to reduce reflectance to less than .5% average from 425 to 700 millimicrons per surface. This coating fulfills the spectral and environmental requirements of MIL-C-14806A. See Specification 1081, Coating No. 527.

Infrared Region

Low Reflection Coatings can be applied to IR transmitting materials tailored to minimize reflectivity up to 15 microns. Coating materials are selected to give optimum results for varying indices.

Angle of Incidence

Low reflection coatings are tailored for highest efficiency at normal incidence and will maintain satisfactory reducing reflections at angles of incidence up to 30°. Low reflection coatings can be tailored to optimum efficiency at other specified angles of incidence.

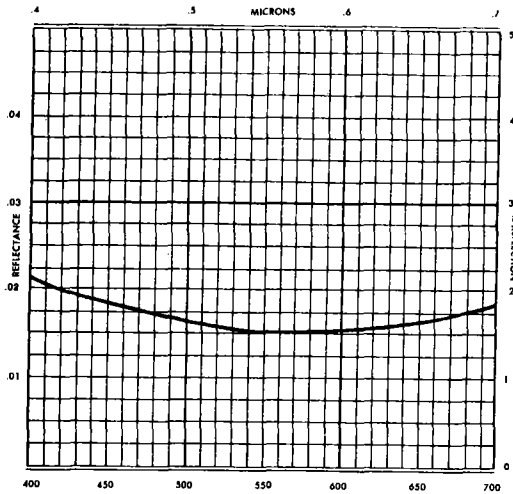
Hardness

No evidence of film removal or film abrasion shall be visible to the eye when any one or all of the following tests are applied:

- (a) The coated optical element shall be carefully washed first in a solution consisting of one (1) ounce of sulphated alcohol, one (1) ounce 15 Baume normal ammonium hydroxide, and one (1) gallon water; then cleaned in acetone or grain alcohol and dried with lens tissue or soft cloth.
- (b) A thick paste of U.S.P. precipitated chalk and water shall be applied to the coating and allowed to dry, and then wiped off with a soft cloth.
- (c) A pad of clean, dry cheesecloth (previously laundered) ¾ inch in diameter, ½ inch thick, bearing with a force of one pound on the coating shall be rubbed across the coated element in any direction 150 times.

Note: During the above tests, care should be exercised to prevent contaminating abrasives contacting the coated surface causing slight streaks.

**Regular Low Reflection Coating No. 525
(MIL-C-675A)**



Wave length in millimicrons

*When the coated element is used at angles other than normal, curve peaks will shift toward shorter wave lengths (down scale). This variation is dependent on degree of angularity from normal incidence.

SPECIFICATION NO. 1079

Reflection

The Low Reflection coating shall have less than 1.5% reflectance at minimum point on substrate with index of refraction of 1.52.

SPECIFICATION NO. 1080

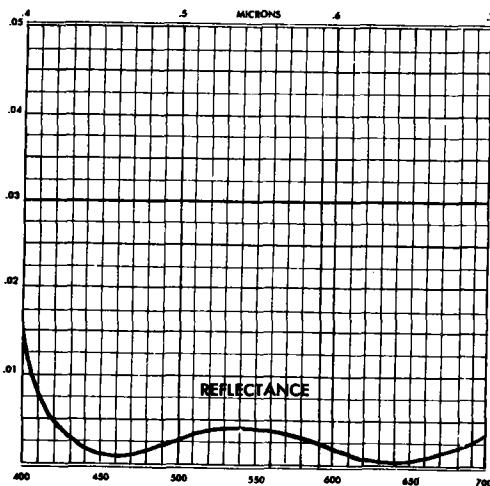
Reflection

The following table indicates the reflectance from a single surface of a substrate having indices of refraction within the range of 1.47 - 1.55, coated with our SLR coating:

Wavelength Range Nanometers	Reflectance Percentage for Angle of Incidence Shown		
	0° to 15° Incl.	Absolute	30°
450 to 625 incl.	0.6	1.0	1.0
500 to 600 incl.	0.35	0.6	0.6
450 to 625 incl.	0.40	0.8	0.8

**HEL R - Hi-Efficiency Low Reflection Coating No. 527
(MIL-C-14806A)**

Spectrophotometric curve shown in the visible region is measured at 15° from the normal incidence.

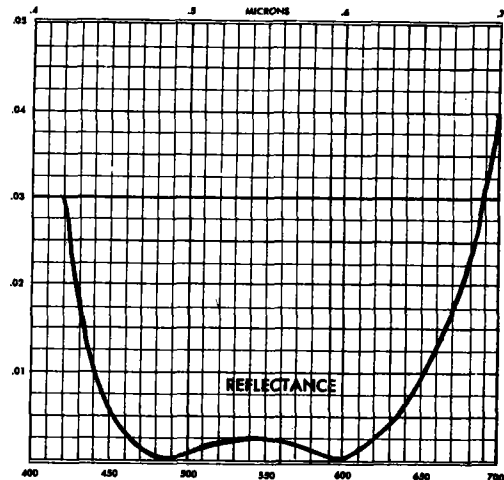


Wavelength in Nanometers

When the coated element is used at angles other than 15° incidence, curve peaks will shift. For angles greater than 15°, the curve peaks will shift down scale.

SLR - Special Low Reflection Coating No. 526

Spectrophotometric curve shown in the visible region is measured at 15° from the normal incidence.



Wavelength in Nanometers

*When the coated element is used at angles other than 15° incidence, curve peaks will shift. For angles greater than 15°, the curve peaks will shift down scale.

SPECIFICATION NO. 1081

Reflection

The following table indicates the reflectance from a single surface of a substrate having indices of refraction within the range of 1.47 - 1.55, coated with our HEL R coating:

Wavelength Range Nanometers	Reflectance Percentage for Angle of Incidence Shown		
	0° to 15° incl.	Absolute	30°
450 to 675 incl.	0.6	1.0	1.0
500 to 620 incl.	0.35	0.5	0.5
425 to 700 incl.	0.5	0.6	0.6

Light Absorption

Within the wavelength range of 425 - 700 millimicrons, light loss in the coating shall not exceed the following limits per surface.

Maximum average absorption	0.5%
Maximum absolute absorption	2.0%
Maximum diffuse reflectance	0.1%

SELECTIVE INTERMETALLIC COMPOUND SURFACES

Teuvo Santala

Texas Instruments Incorporated
Attleboro, Mass. 02703

Certain intermetallic compounds in which aluminum is one of the component metals have a highly porous surface structure when they are formed by reacting the component metal layer thermally in solid state. Figure 1 shows scanning electron microscope pictures of three different intermetallic compound surfaces for which the compound forming conditions were the same. All three surfaces exhibit high solar absorptance, but the infrared emittance of the Al-Ni is significantly lower (Figure 1).

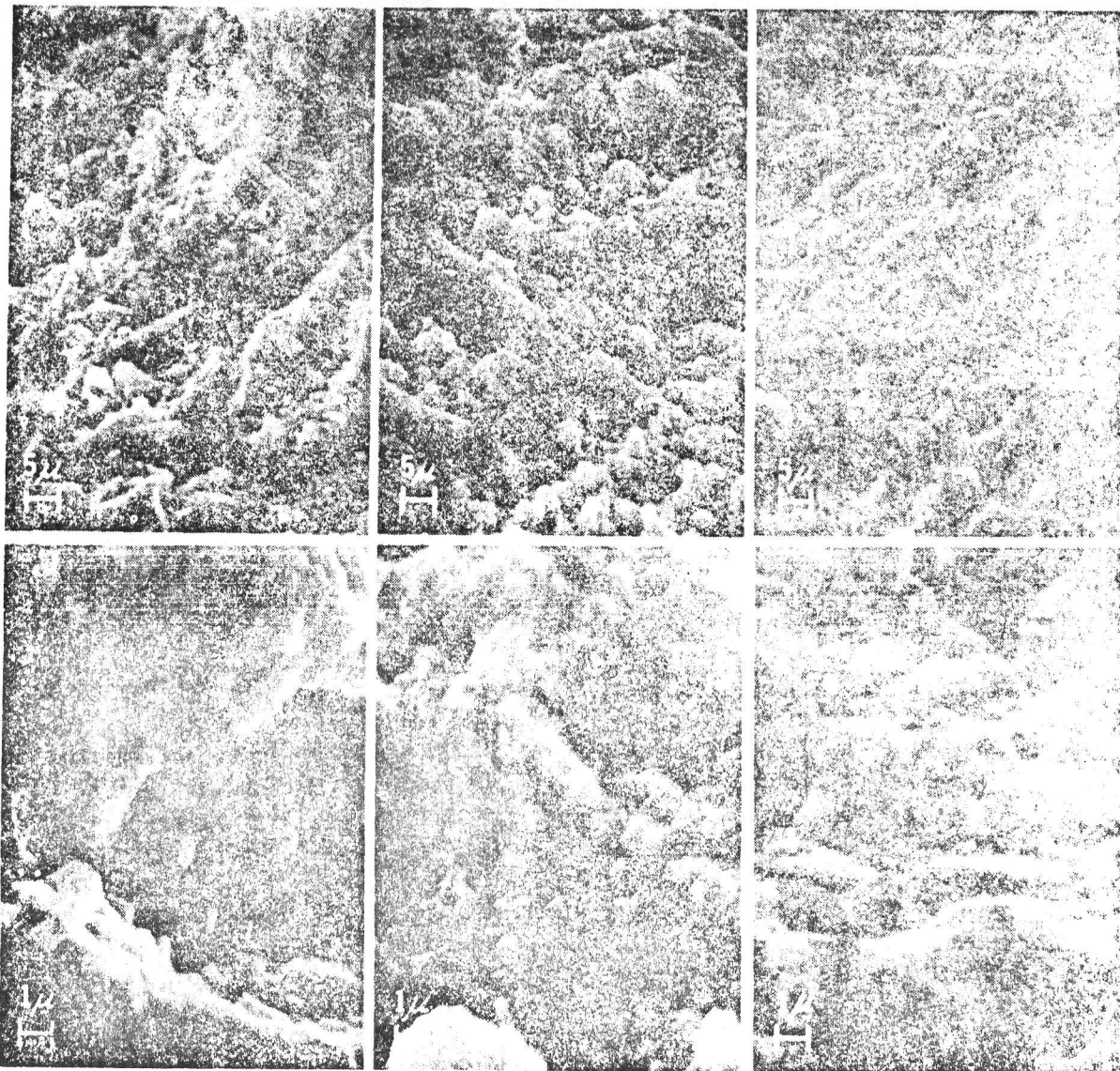
The SEM pictures at 5000X show that the dimensions of the fine structure of each compound is of the same magnitude as the wave length range of the incident solar radiation, and these surfaces absorb as black body cavities. The exact reason for the lower infrared emittance of the Al-Ni intermetallic compound has not yet been determined, but the fine structure of its surface is porous (Figure 1c) rather than dendritic as it is for the Al-Fe and Al-Cr surfaces (Figures 1a and 1b). Consequently, it appears that the Al-Ni surface radiates in the infrared wave length region as a smoother surface than either Al-Fe or Al-Cr.

The porous surfaces were impregnated with thin layers of various polymers such as polyimide and methyl-metacrylate, and with clear glass enamels, which are transparent to solar radiation and generally opaque to infrared radiation to evaluate if the coatings would cause a "greenhouse" effect and thus influence the selectivity of the absorption surface. The solar absorptance was reduced only by an insignificant amount, but the infrared emittance of the impregnated surfaces approached values which were characteristic of those of the impregnating media and consequently the selectivity was improved only in the cases where the initial emittance was high.

Samples of impregnated Al-Fe and Al-Ni surfaces have been subjected to environmental testing for five months in a typical flat plate collector with one glass pane and for three months to an accelerated durability testing in which the relative humidity at room temperature is cycled between 10-20% and 100% every eight hours. Visually observable changes were not detected in any of the Al-Ni intermetallic compound surfaces after either testing. The Al-Fe compound surfaces started to show macroscopic rust spots after the three months accelerated testing, but visually observable changes were not detected after the five months exposure in the flat plate collector enclosure.

Work is in progress to incorporate these intermetallic compound surfaces into a composite metal tube-in-sheet

collector plate to test their collection performance and to further evaluate their durability.



a) Al-Fe

$\alpha \sim 0.98$

$\beta \sim 0.55$

b) Al-Cr

$\alpha \sim 0.99$

$\beta \sim 0.59$

c) Al-Ni

$\alpha \sim 0.95$

$\beta \sim 0.28$

Figure 1. Scanning electron microscope pictures of three intermetallic compound surfaces. Upper row $\sim 1000X$, lower row $\sim 5000X$.

Dr. Santala is the Branch Manager of Metallurgical Research at Texas Instruments Incorporated, Attleboro, Mass.

